



Protection of Dental Materials: Mucin Layer Growth Kinetics & Properties and Their Influence on Lubrication

Pravin Smart^{*}, Michael Bryant

School of Mechanical Engineering, University of Leeds

ARTICLE INFO

Keywords:

Mucin adsorption kinetics
Bio-lubrication
Mucin layers
QCM-D
Dental tribology
PGM

ABSTRACT

The formation of mucin layers on dental materials are intrinsic to maintaining a healthy oral cavity. Of interest to this study is the absorption-property-lubrication ability of surface bound mucin layers on to hard dental surface akin to those observed in oral salivary pellicles. QCM-D experiments examined the growth of these mucin layer overtime. Pseudo First Order, Pseudo Second Order and Elovich kinetic adsorption models were applied to gain a greater insight into the adsorption process. As lubrication on teeth is an important property of oral lubrication, a micro-tribometer was used to assess the lubricity of surfaces over a range of normal loads. Mucin layers grew with an initial rapid phase followed by a second slower adsorption phase which followed Pseudo First Order or Elovich adsorption kinetics on hydroxyapatite and gold surfaces respectively. Enhanced lubrication was seen when hydroxyapatite and mucin were used demonstrating the chemical nature of the underlying surfaces is important in establishing effective mucin films. The formation of mucin layers was attributed to the surface composition driving the adsorption process and subsequent viscoelastic properties of these layers. Hydroxyapatite was important in promoting enhanced mucin lubricity and that mucin boundary lubrication was related to the viscosity and shear modulus of mucin layers.

1. Introduction

Xerostomia, also known as dry mouth, is a chronic condition related to the hypofunction of salivary glands, reducing salivary flow and/or compromising salivary composition [1]. It has been estimated that the overall prevalence of dry mouth is 22% of the population, which increased in elderly groups [2]. It can be attributed to certain medications, irradiation of the head or neck from cancer therapies, diseases including Sicca Syndrome (Sjögren's syndrome) and Type 1 Diabetes, psychological conditions, age and gender [3–6]. This condition can be a particular nuisance when it comes to dental hygiene, increasing the prevalence of tooth decay, dental caries, demineralisation, and tooth enamel loss in patients presenting xerostomia symptoms [6]. This highlights the importance of saliva when it comes to the protection of dental tissues.

Saliva possesses numerous qualities which are crucial for protection and upkeep of the oral environment. Regarding dental tissues, saliva's role can be subdivided into three main areas of protection: preventative defences, active defences and reformation. The preventative defences relate the film forming abilities of saliva, active defences relate to

saliva's lubricating and natural buffering abilities, while reformation is related to the remineralisation of dental tissues after mastication and acidic challenges [7–14]. It has been documented that this layer forms via protein-surface electrostatic interactions, creating a layer which acts as a chemical diffusion layer and boundary lubricating film [7–11]. This layer effectively reduced friction between dental and oral surfaces while also controlling the movement of calcium and phosphate ions from the enamel surfaces [9,14,15].

The properties of salivary proteins, the oral environment and the surfaces have an impact on the film formation process and subsequent viscoelastic behaviour of adsorbed protein layers. Saliva adsorption studies have previously examined the pathways to the formation of a pellicle on a range of surface materials. Quartz crystal microbalance with dissipation monitoring (QCM-D) studies have examined the growth of salivary films on a range of surfaces including: gold, hydroxyapatite, zirconia, titania, silica and PDMS [16–20]. Notable changes in adsorption rate, adsorption behaviour (monophasic or multiphasic), layer thickness, layer viscoelasticity and the overall layer retention when subjected to different rinse solutions have been observed [16]. Furthermore, the surface's chemical composition, heterogeneity,

^{*} Corresponding author.

E-mail addresses: mn12p2s@leeds.ac.uk (P. Smart), M.G.Bryant@leeds.ac.uk (M. Bryant).

potential, polarity and topography are factors which govern interactions with these proteins [18,21,22]. Therefore, protein and surface characteristics alike need to be scrutinised to engineer a particular protein layer within a given environment.

Electrostatic forces, hydrophobic and secondary adsorption interactions (i.e. Van der Waals forces and hydrogen bonding) have been suggested to be the main driving forces for salivary protein adsorption [16,17,23–25]. Studies that have considered human saliva or isolated salivary protein alone (i.e., mucin, lysosome, lactoferrin, statherin and other proline rich proteins) demonstrate progressive adsorption via these pathways on various surfaces as seen by QCM-D and ellipsometry [16–20,26]. Gold, silica and titanium surfaces are more commonly used to examine saliva adsorption, compared to hydroxyapatite surfaces which are more akin to the surface composition of tooth enamel. A combination of physisorption and chemisorption pathways are also observed for gold surfaces [16–18]. However, it is unclear to the order in which adsorption might occur. There are few studies which further explore the adsorption of saliva or saliva substitutes by applying known kinetic adsorption models, specific to physisorption and chemisorption pathways. These models may provide further insight into the adsorption process over time and aid in the identification of surface dependant adsorption pathways.

Mucin, a glycoprotein component of saliva, has been previously examined as a potential additive to artificial saliva substitutes [27–29]. It is a multifunctional component of saliva which possesses boundary lubricative, viscoelastic, anti-bacterial and digestive properties [10,30,31]. These characteristics make it a viable component for an artificial saliva substitute; however, it is important to assess how this component forms protective layer alone. Studies have shown that mucin within an artificial lubricant adsorb to surfaces, reducing surface wear by influencing the wear mechanisms [27,32]. Reductions in abrasive wear and the prevention of adhesive wear mechanisms indicate the structural and lubrication properties of mucin-surface layers are important when it comes to surface protection [32]. It has been suggested that this relates to an aqueous boundary lubrication regime that depend on the adsorbed protein layer's "structural softness" (viscoelastic properties) and the layer's ability to retain water [33,34]. It is important for an artificial saliva to engineer a protective layer upon application to dental surfaces, similar to what is observed in vivo with saliva. The mechanisms of mucin only adsorption is not yet fully understood and it is not fully clear how the degree of mucin layer viscoelasticity directly influences lubrication at this scale. This study therefore aimed to:

- Further examine mucin adsorption pathways by combining data acquired from a QCM-D with a few known kinetic adsorption models; and
- Provide a direct link between QCM-D observations and tribological outcomes.
- Understand implications of commercial mucin purification and perturbing salt molecules on the above.

2. Materials and Methodology

2.1. Mucin Layer Growth Solution

Porcine Gastric Mucin (PGM, Sigma Aldrich) was used to simulate salivary mucins to assess its ability to self-engineer a surface film when used as received, with additional purification, and with perturbing salts. PGM was chosen as a benchmark molecule to assess the link between observed mucin layer properties and its tribology. PGM has been used in several studies in the field of dental wear and corrosion, in addition to being a component in commercial saliva substitutes [28,29,35–39] and served as a suitable benchmark to assess adsorption kinetics in relation to layer properties and lubrication behaviour. 0.2% w/v mucin solutions were made up from 100 mL deionised water or phosphate buffer saline

(PBS) solution and 0.2 g of as received or purified PGM. This ensured that the protein layers could be analysed as received and compared to further purified PGM derivatives, both with and without PBS salts. MilliQ water (>18 M Ω purity) and PBS solutions were used as a rinse solution for QCM experiment i.e. MilliQ rinse for PGM in deionised water and PBS rinse for PGM in PBS. Purification of PGM was achieved by dissolving 300 mg PGM in 10 mL deionised water followed by dialysis in 100 kDa molecular weight cut-off membrane (Spectrum Laboratories, USA) against deionised water for a week, followed by lyophilisation. The acronyms PGM and PGM + PBS refer to "as-received" PGM and PGM with added PBS salts, while pPGM and pPGM + PBS refer to the same solutions using purified PGM. Purified PGM was produced according to the method published by Xu et al. [40].

2.2. Quartz Crystal Microbalance

Quartz crystal microbalance with dissipation monitoring (QCM-D) on a Qsense Analyzer (Biolin Scientific/Qsense, Sweden) was utilised to assess the adsorption of mucin layers onto surfaces. 5 MHz fundamental frequency 14 mm Cr/Au gold (Au) (Quartzpro, Sweden) and hydroxyapatite (Hap) QSX 327 HA (Biolin Scientific/Qsense, Sweden) sensors were used to compare surface specific differences in mucin layers. All sensors were new and unused prior to testing. Prior to sensor mounting gold sensors were sonicated in MilliQ water for 10 min at 30 °C followed by drying under a nitrogen gas flow. Hap sensors were submerged in 99% ethanol for 30 min, followed by thorough rinsing in MilliQ water and drying under a nitrogen gas flow.

The QCM-D directly measured two variables, the changes in resonant frequency and the changes in dissipation, a measure of the energy lost during one oscillation and the energy stored. The changes in frequency relate to the changes in adsorbed mass on the sensor's surface over time i.e. an increase in mass on the sensor's surface would be sensed as a drop in the resonant frequency harmonics by the QCM-D. Simultaneously, the changes in dissipation relate to the rigidity of the formed surface layer over time. If the change in dissipation (ΔD) was ≈ 0 for all resonant harmonic frequencies (a.k.a. overtones), then it could be assumed that the layer was thin and rigid, thus the Sauerbrey equation would adequately model the layer's thickness properties. However, if $\Delta D > 0$ and the overtones were more spread out then layer would show viscoelastic behaviour and a viscoelastic model must be used to accurately predict thickness and viscoelastic properties [41].

In this study, it was determined that the layers were in fact viscoelastic, as $\Delta D > 0$ was observed, in behaviour and were therefore modelled using the Broadfit model of the Dfind software (Biolin Scientific, Sweden). The Broadfit model followed a Voight viscoelastic model which describes viscoelasticity as a complex shear modulus accounting for the storage and loss moduli [42]. The storage modulus is independent of the applied frequency whereas the loss modulus is linearly dependent on frequency [43]. It was assumed layers that formed behaved like a polymer where structure was maintained with no observed flow. It was also assumed that any formed layers covered the entire area of the sensor and were uniform in density and thickness. Further assumptions are detailed in Voinova et al. [42]. The frequency dependent viscoelastic properties parameter was included during the modelling process to provide more realistic results.

A peristaltic pump was used to simulate the flow of saliva throughout tests at a rate of 0.4 mL per minute and the unit cell temperature was set to a constant 25 °C for all tests. Two aspects of the mucin layer were examined. A growth phase using a 0.2% mucin solution for 30 min followed by a rinse phase with MilliQ water. The rinse phase assessed the robustness of the layer once the growth solution was removed.

2.3. Adsorption and Desorption Kinetics Modelling

The adsorption of mucin onto these surfaces was examined further with the application of kinetic adsorption models by comparing the fit of

3 models; Pseudo First Order (PFO), Pseudo Second Order (PSO) and Elovich. This allowed the rates of mucin adsorption to be investigated with a possible insight into the adsorption interactions. Solute concentrations and flow rate remained the same throughout QCM-D experiments and this allowed for more focus on the interactions between mucin and surfaces. The PFO and PSO model are commonly used in the literature for adsorption kinetics [44]. Adsorption may be dominated by either physisorption, i.e. weak bonding via electrostatic interactions, hydrogen bonding, hydrophobic interactions and Van der Waals forces, or, chemisorption, i.e. stronger chemical bonding involving electron sharing or transfer via covalent or ionic bonding. Furthermore, multilayers are more associated with physisorption whereas monolayers are linked to chemisorption [45]. These PFO and PSO models indicate whether adsorption is more inclined towards physisorption and chemisorption respectively and are modelled as follows:

2.3.1. The PFO Model

The PFO model, aka Lagergren model [46], describes the adsorption capacity of adsorbate to adsorbent as described in Eq. (1).

$$\frac{dq_t}{dt} = k_1(q_e - q_t) \quad (1)$$

Where q_t is the mass adsorbed onto the surface at time t , q_e is the mass adsorbed at equilibrium and k_1 is the rate constant. This was integrated using the boundary conditions $q_t = 0$, $q_t = q_e$, $t = 0$ and $t = t$ for Eq. (1) to be re-written as Eq. (2).

$$q_t = q_e(1 - e^{(-k_1 t)}) \quad (2)$$

The PFO desorption model describes the desorption as a function of the adsorbed species as described by Eq. (3), where k_{D1} is the desorption rate constant [47].

$$q_t = q_e e^{(-k_{D1} t)} \quad (3)$$

2.3.2. The PSO Model

The PSO model describes the rate of adsorption as proportional available active sites on the surface. The amount of adsorbate adsorbed on the surface acts as the driving force for adsorption as over time the number of active sites reduces, reducing the adsorption rate. This is described in Eq. (4).

$$\frac{dq_t}{dt} = k_2(q_e - q_t)^2 \quad (4)$$

Using the same boundary conditions used for the PFO model, this was integrated and rearranged into Eq. (5).

$$q_t = \frac{k_2 q_e^2 t}{k_2 q_e t + 1} \quad (5)$$

This model was used to describe valance forces through the sharing of electrons between adsorbent and adsorbate and ion exchange [46].

The PSO desorption model describes the desorption as a function of the adsorbed species on the surface as described by Eq. (6), where B is a constant and k_{D2} is the desorption rate constant [47].

$$q_t = q_e \frac{1}{B + k_{D2} t} \quad (6)$$

2.3.3. The Elovich Model

The Elovich model assumes the surface to be energetically heterogeneous with no interactions between adsorbed species. The model provides a good fit to heterogeneous surfaces which favour chemisorption as the dominant mechanism of surface adsorption and is described in Eq. (7).

$$\frac{dq_t}{dt} = \alpha e^{-\beta q_t} \quad (7)$$

Where α is the initial adsorption rate and β is the desorption constant and is related to the extent of surface coverage and activation energy for chemisorption [48,49]. Like before this equation is integrated with the same boundary conditions as for the PFO and PSO model and is re-written in Eq. (8).

$$q_t = \frac{1}{\beta} \ln(t) + \frac{1}{\beta} \ln(\alpha\beta) \quad (8)$$

The coefficient of determination, R^2 , adjusted R^2 , adj R^2 , and Chi squared, χ^2 , error functions were examined to determine which kinetic model best fitted the experimental data.

2.4. Friction Analysis on QCM Sensors

A microtribometer (Anton Paar, NTR³) was used to assess the sliding friction on both Au and Hap QCM sensors post mucin deposition. A reciprocating ball on flat configuration was used and tests were performed in solution against a Ø3 mm Yttria stabilized Tetrahedral Zirconia Polycrystalline (Y-TZP) ball. The frictional force (F_t) was measured over varying loads and was controlled with a piezo actuator. Normal loads (F_n) between 50 and 500 μ N were applied, starting at 50 μ N and increasing by 50 μ N every 200 cycles (10 increments in total). Hertzian contact pressures were calculated to be within 15–60 MPa over the duration of a single test run. The cycle frequency was constant throughout testing at 1 Hz and the sliding distance per cycle was 1000 μ m resulting in a sliding speed of 1 mm/s. A sinusoidal wave displacement profile was used and an acquisition frequency of 400 Hz was applied for all load increments. To determine the mean F_t for each sliding cycle, a frictional force vs linear position loop was used, taking an average of the frictional force during steady state sliding for the forward and reverse directions as presented in Fig. 1. The middle 20% of the friction loop was used to determine the friction force, highlighted by the blue shaded region.

The coefficient of friction (μ) was determined by the gradient of the mean F_t vs F_n curve which follows Amonton's first law according to Eq. (9), where C is an unknown constant of related to interfacial adhesion forces. Three repeats were performed for deionised water and the 0.2% mucin solution on each sensor material. Tests were conducted after 30 min of exposure to all growth and rinse solutions used for the QCM experiments. Sensors were then removed and tests were performed in 0.1 mL of the related test solution.

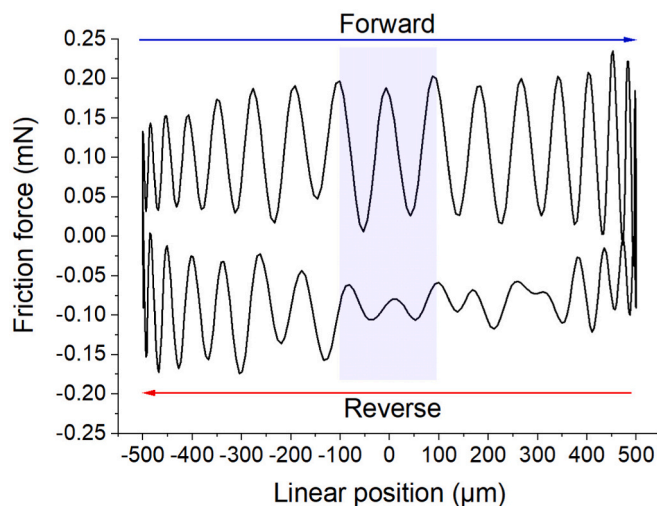


Fig. 1. Hysteresis loop showing frictional force, F_t , vs linear position. The blue and red arrows represent the forward and reverse trace respectively and the shaded region shows the area of steady state sliding used to determine a cycle's mean F_t . (For interpretation of the references to colour in this figure legend, the reader is referred to the web version of this article.)

$$F_t = \mu F_n + C \quad (9)$$

2.5. Data Analysis and Statistics

Data was collected in triplicate for each surface material and test solution ($n = 3$). All QCM-D data was processed by and exported from the Dfind software (Biolin Scientific, Sweden). Mean and standard deviation (SD) calculations for modelled layer properties were performed using Excel (Microsoft, USA). Student t -tests were also performed assuming unequal variances and a two-tail distribution to determine whether differences between results were significant ($p < 0.05$).

3. Results & Discussion

3.1. Mucin Layer Growth Behaviour and Properties on Gold and Hydroxyapatite Surfaces

Frequency and dissipation data was processed to determine the average layer properties during the end of both growth and rinse phases. Fig. 2 shows the average properties and standard deviation bars for all PGM solution growth phases and rinse phases for gold and Hap sensors ($n = 3$ per sensor material).

3.1.1. Layer Thickness Comparison

At the end of the growth phase the average PGM layer thickness on gold and Hap was 29.73 ± 2.10 nm and 23.2 ± 4.69 nm, respectively, increasing to 33.62 ± 2.51 nm and 32.10 ± 1.52 nm in the rinse solution ($p > 0.05$ for both). This is indicative of layer swelling as the solution environment no longer contained PGM which created an osmotic pressure difference for the movement of water into the layer [50]. This behaviour was not observed during the rinse phase of the other PGM solution variants. PGM + PBS and pPGM + PGM solutions presented layers with a similar thickness, with 25.62 ± 10.37 nm and 22.21 ± 4.88 nm on gold and 20.64 ± 2.89 nm and 22.92 ± 3.03 nm on Hap. On the other hand, pPGM presented the smallest layer thickness on both gold and Hap, with 13.32 ± 0.38 nm and 15.42 ± 9.85 nm respectively. This suggested that both additional salts and purification steps influenced build up protein layers on both surfaces. Significant differences were observed during the growth phase layer thicknesses between PGM and pPGM on gold (13.32 ± 0.37 nm with $p = 0.031$), and PGM layers on Hap compared to gold ($p = 0.049$). During the rinse phase, significant differences were observed only between PGM and pPGM layers on gold (10.79 ± 0.36 nm with $p = 0.022$).

3.1.2. Layer Shear Modulus Comparison

Significant differences between the shear modulus properties of layer were observed on both gold and Hap surfaces during the growth phase. On gold, the pPGM layer presented a shear modulus of 100.18 ± 12.85 kPa, which was significantly larger than other layers on gold with shear moduli of 41.98 ± 3.34 kPa for PGM ($p < 0.001$), 36.08 ± 14.80 kPa for PGM + PBS ($p < 0.001$) and 48.80 ± 5.05 kPa for pPGM + PBS ($p = 0.002$). On Hap, the PGM layer presented a similarly larger shear modulus of 116.16 ± 21.12 kPa, which was also significantly larger than other layers grown on Hap, with shear moduli of 38.51 ± 5.34 kPa for PGM + PBS ($p < 0.001$), 21.25 ± 10.53 kPa for pPGM ($p < 0.001$) and 21.89 ± 5.89 kPa for pPGM + PBS ($p < 0.001$). During the rinse phase, the shear moduli were generally shown to increase on gold surfaces, and decrease on Hap.

3.1.3. Layer Viscosity Comparison

As for the layers' viscosity properties, significant differences were observed between pPGM layers on gold, with a viscosity of 2495.19 ± 131.70 μ Pa.s compared to PGM with 1256.95 ± 38.75 μ Pa.s, PGM + PBS with 1320.41 ± 235.84 μ Pa.s and pPGM + PBS with 1531.53 ± 26.68 μ Pa.s ($p < 0.001$ for all). During the rinse phase, the pPGM layer

viscosity increased significantly to 2924.72 ± 153.96 μ Pa.s ($p = 0.037$), while the viscosities on other gold layers were similar to their growth phase viscosities. On Hap, the pPGM layer presented significant differences to other Hap layers' viscosities, with a lower viscosity of 895.90 ± 510.75 μ Pa.s compared to PGM with 2005.59 ± 89.81 μ Pa.s ($p < 0.001$), PGM + PBS with 1582.57 ± 91.64 μ Pa.s ($p = 0.033$) and pPGM + PBS with 1359 ± 54.03 μ Pa.s ($p = 0.033$). When layer viscosities were compared between materials, differences between both PGM and pPGM layers were significant, with $p = 0.011$ and $p < 0.001$ respectively.

3.1.4. Layer Properties in Relation to the Literature

The calculated viscosity shown in Fig. 2 c) is similar to what has been shown in a previous study which examined the formation of salivary films on different dental materials, using untreated and filtered whole human saliva [16]. Whole saliva layers on gold displayed a shear modulus of 14.2 kPa, a viscosity of 1500 μ Pa.s and a thickness of 23.7 nm whereas whole saliva layers on hydroxyapatite displayed a shear modulus of 170 kPa, a viscosity of 2700 μ Pa.s and a thickness of 9.8 nm [16]. These differences were attributed to the stronger attachment of salivary proteins to the hydroxyapatite surface, forming a stiffer layer that potentially forms with additional crosslinking between mucin and calcium ions in saliva [51]. It is not suggested how this relates to the surface composition. Mucin is a high molecular weight molecule and is the third most abundant protein within whole human saliva accounting to between 4.5 and 17.5% of the total protein content [52]. The similarities in the viscoelasticity of protein layers formed by saliva and the mucin layers may pertain to the presence of mucin [53]. What this suggests is that mucin plays a large role on the viscoelasticity on the formation of a salivary layer. In the current study, the viscoelastic properties of PGM + PBS and pPGM + PBS layers on gold, and PGM layers on hydroxyapatite were closest to the properties observed on whole human saliva layers on the corresponding surfaces [16]. Differences can be attributed to the fact that in the current study, PGM was examined in the absence of potential precursor salivary proteins, with existing inorganic salts and protein impurities [54]. For non-purified PGM solutions, this could be thought to mimic the adsorption pathways of saliva where smaller sized protein impurities or mucin fragments initiate the adsorption process onto both surfaces, followed by larger mucin polymers or aggregates that replace or co-mingle with the surface bound proteins [55].

Another study focusing on mucin only films examined the growth of purified bovine submaxillary mucin (BSM) onto gold surfaces compared to purified type III PGM [56], where a more viscous PGM layer formed on gold compared to a more elastic BSM layer. The differences may relate to larger proportion of sialic acid groups within a BSM monomer compared to PGM, 9–24% carbohydrate mass vs 0.5–1.5% respectively [56,57]. This essentially means that the central region of BSM is more hydrophilic relative to PGM, which may promote additional H bonding and crosslinking within the layer's structure [56]. This is shown to influence thin film structural properties onto PDMS surfaces where a more elastic film/less viscous BSM film is observed and a more viscous/less elastic film was observed for PGM [56]. No comparisons were made between the as-received BSM and PGM compared to their purified counterparts regarding layer growth [56], however in a different analysis it was confirmed that the purification process had removed smaller species, minimising the impact of non-mucinous protein impurities. Impurity removal in the current study was shown to largely influence the viscoelastic properties of the layers, with surface composition affecting the purified PGM layers differently. Both surfaces presented thinner pPGM layers compared to crude PGM, however shear modulus properties of the pPGM layers increased on gold, but reduced in hydroxyapatite layers as shown in Fig. 2 a) c) and d).

3.1.5. Qualitative Assessment of Layer Property Change

Fig. 3 shows the change in dissipation (ΔD) plotted against the change in frequency (Δf), which provides a qualitative evaluation of the

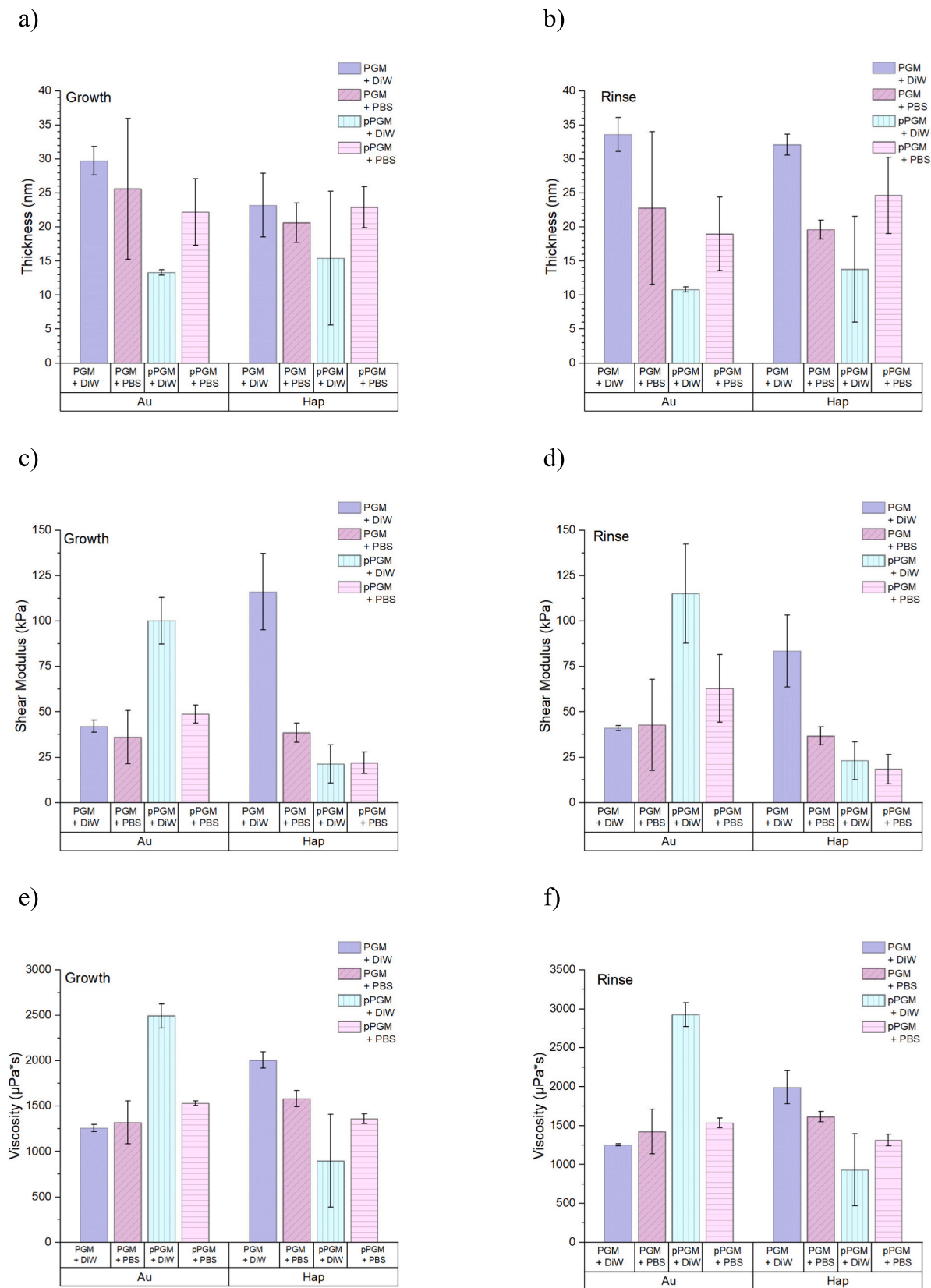


Fig. 2. Mean layer properties with SD bars calculated from ‘Broadfit’ model comparing gold and Hap sensors under PGM, PGM + PBS, pPGM, and pPGM + PBS conditions; a) Thickness – growth phase, b) Thickness – rinse phase, c) Shear modulus – growth phase, d) Shear modulus – rinse phase, and e) Viscosity – growth phase, f) Viscosity –rinse phase. (For interpretation of the references to colour in this figure legend, the reader is referred to the web version of this article.)

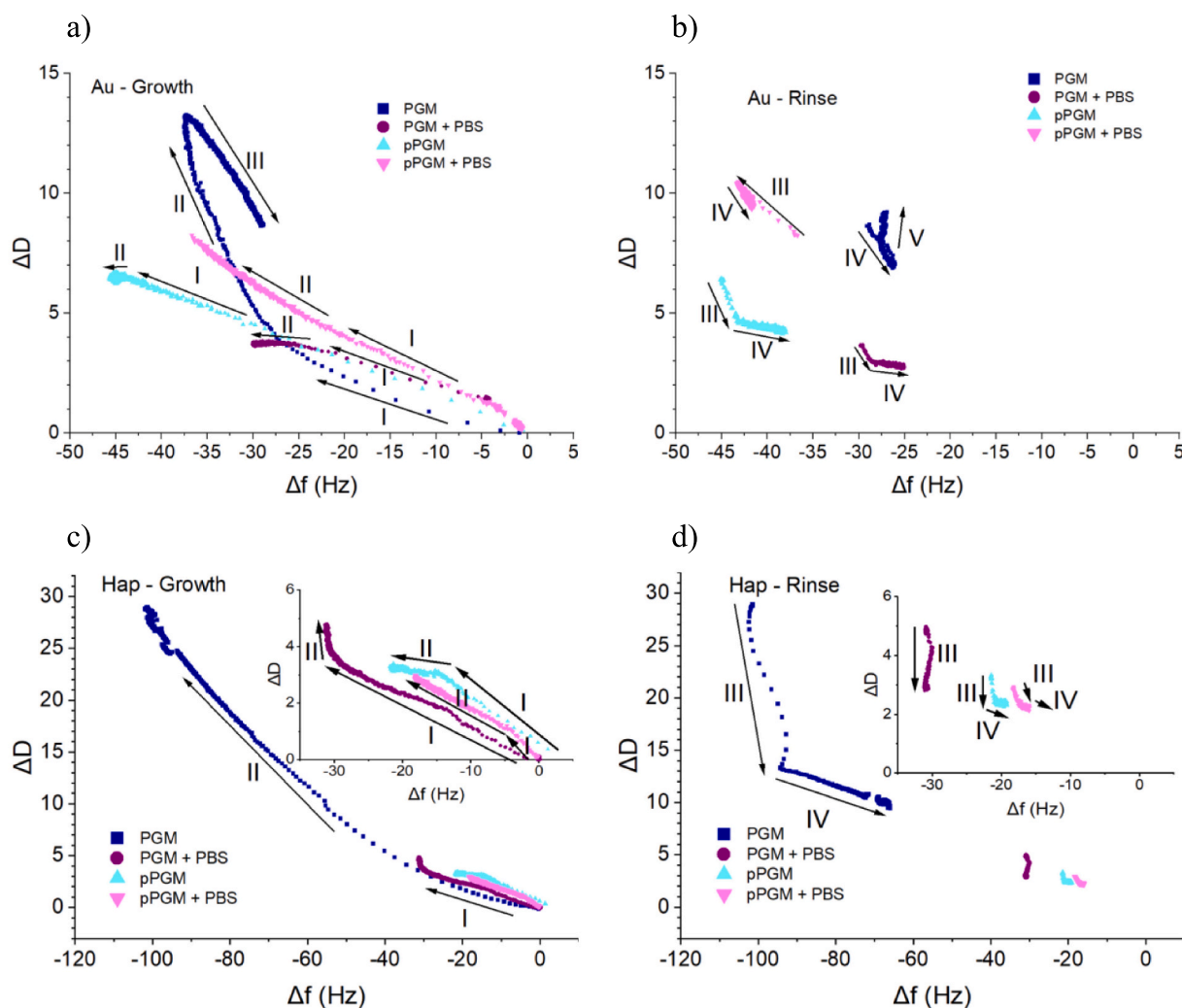


Fig. 3. Qualitative assessment of PGM layer viscoelasticity by comparing ΔD vs Δf . Layers: a) gold – growth phase, b) gold rinse phase, c) Hap growth phase and d) Hap rinse phase. Arrows indicate the how layer response changes with increasing time, while roman numerals indicate regions of interest relating to adsorption, desorption, swelling or shrinking. (For interpretation of the references to colour in this figure legend, the reader is referred to the web version of this article.)

viscoelastic and structural properties of the PGM layer in terms of sensor dissipation per unit mass adsorbed. A steeper $\Delta D/\Delta f$ gradient indicates increasing dissipation with additional mass which is characteristic of a more dissipative, softer and viscous layer [16,58]. On the other hand, a flatter gradient indicates a more rigid and elastic layer [16,58]. Roman numerals in Fig. 3 relate to stages in the layer's development while arrows indicated the direction of change with respect to time.

On gold, multiple adsorption process were observed with PGM, PGM + PBS, pPGM and pPGM + PBS, show in Fig. 3 a). PGM's initial stage on gold, arrow I, indicated a more elastic and rigid layer formed before following a steeper gradient with arrow II, which suggested a softening of the layer prior to conformational changes at the end of the growth phase, arrow III. This is indicative of the subsequent desorption of loosely bound mucin to the established adsorbed layer and restructuring of the remaining mucin which has been previously observed [34,59]. The reverse was observed for PGM + PBS and pPGM, with a steeper gradient initially, arrow I, followed by a flatter line with arrow II. This suggested that the layers started out soft initially and begin to exhibit more elastic behaviour as more mass adsorbs to the surface. pPGM + PBS followed a similar behaviour to PGM, but without the conformational change. On Hap, PGM and PGM + PGM layers followed a similar growth pattern to arrow I and II for PGM layer growth on gold, shown in Fig. 3 c). Furthermore, PGM layer on Hap presented a larger overall

dissipation and frequency change compared to all layer growth, however the rate of change was comparable. Interestingly, the reverse was observed with pPGM and pPGM + PGM adsorption to Hap, with a steeper initial phase, arrow I, compared to a flatter second phase, arrow II. These differences were attributed to the removal of impurities in the PGM solutions which may have altered the adsorption pathways.

When the rinse is presented, Fig. 3 b), there is an increase in frequency and reduction in the dissipation as loosely bound molecules are removed from the PGM layer on gold, shown by arrow IV. This was followed by an increase in the dissipation and slight decrease in the frequency, arrow V, indicating the uptake of the bulk fluid and subsequent layer swelling. Both PGM + PBS and pPGM layers on gold followed a similar trend, with layer structural changes increasing its elasticity, arrow III, follow by conformation changes and layer desorption in shown by arrow IV. The pPGM + PBS layer on gold initially became more dissipative which indicated layer swelling, arrow II, followed by the conformation changes and the removal of the layer, arrow IV. On hap, all solution excluding PGM + PBS followed the same trend, with arrow III indicating a stiffening of the layer followed by layer removal, arrow IV. Only layer stiffening was observed with PGM + PBS on Hap, arrow III.

The mucin layers formed on both surfaces are comparable to the two layered structures which have been observed to form from whole human

saliva [9,16,20,60]. “As received” commercial PGM contains mucins with a size range between 400 nm to 2 μm, is subject to the presence of impurities and has the tendency to form aggregates [61,62]. By not controlling the size of mucin in the growth solution, the adsorption behaviour was hypothesised to mimic the adsorption pathways of saliva where smaller sized mucin monomers initiate adsorption onto both Hap and gold surfaces followed by larger mucin polymers/aggregates that replacing bound mucin on the surface. The removal of some of these impurities was shown to influence the layer properties during adsorption to both surfaces, with and without the addition of PBS salts, which suggested these impurities influenced adsorption pathways and adsorbed layer structure. Saliva adsorption has been shown to follow a 2-phase adsorption process: an initial phase of rapid adsorption of low molecular weight proteins, followed by a slower second adsorption phase where higher molecular weight proteins (i.e. mucin) replace or anchor onto the initial layer [9,16,20,60]. This behaviour can be described by the Vroman effect where the highest mobility proteins arrive to the surface first. These are then replaced by the less mobile proteins with a higher affinity to the surface [55]. This creates a 2 layered structure: a rigid and compacted layer at the surface and a more diffuse layer further out. Fig. 3 a) and c) confirm there are two adsorption phases, but the rate of change is different and dependent on the growth solution used and the surface material.

3.2. Kinetic Adsorption Modelling of Mucin Layer Growth onto Gold and Hydroxyapatite Surfaces

Fig. 4 and Fig. 5 show the change in mass over the growth phase for mucin and purified mucin onto both surfaces respectively. Fig. 4 a) and c) show the first 450 s of mucin adsorption onto gold and hydroxyapatite surfaces with PGM and PGM + PBS solutions respectively, while Fig. 5 a) and c) show the same for purified PGM solutions. The closest fitting kinetic adsorption model, from the three mentioned in the methodology section, is also plotted in the two figures. Output fitting parameters R squared (R^2) and Chi squared (χ^2) are also displayed in each figure. Model fit was determined from how close R^2 was to 1 and which model possessed the lowest χ^2 result.

The two models of interest which emerged to best describe mucin adsorption in this study were the PFO and Elovich kinetic models, of which the calculated model parameters for the crude and purified mucin are presented in Table 1.

3.2.1. Adsorption onto Gold Surfaces

The Elovich model best described the adsorption of as received mucin (PGM) onto the gold surfaces for the entire growth phase, with $R^2 < 0.99$ and $\chi^2 = 2903$, shown in Fig. 4 a). This fit suggested a chemisorption driven adsorption process for mucin monomers onto gold. While the Elovich model is unable to predict definite adsorption mechanisms alone [63,64], the model is indicative of adsorption onto

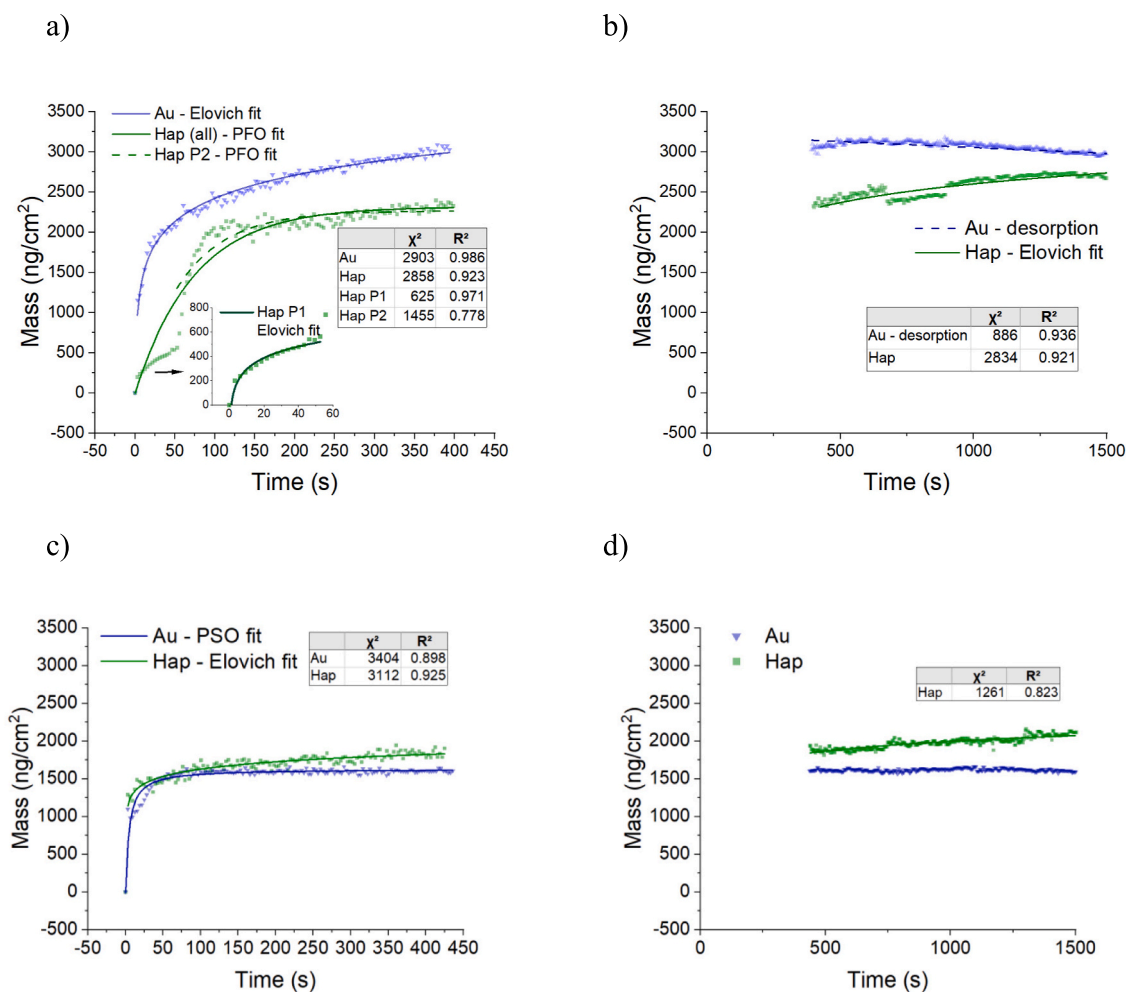


Fig. 4. Best fits of kinetic models for adsorption onto gold and hydroxyapatite for the first stage of layer growth of a) PGM and c) PGM + PBS, and second stage behaviour of b) PGM layers and d) PGM + PBS layers. (For interpretation of the references to colour in this figure legend, the reader is referred to the web version of this article.)

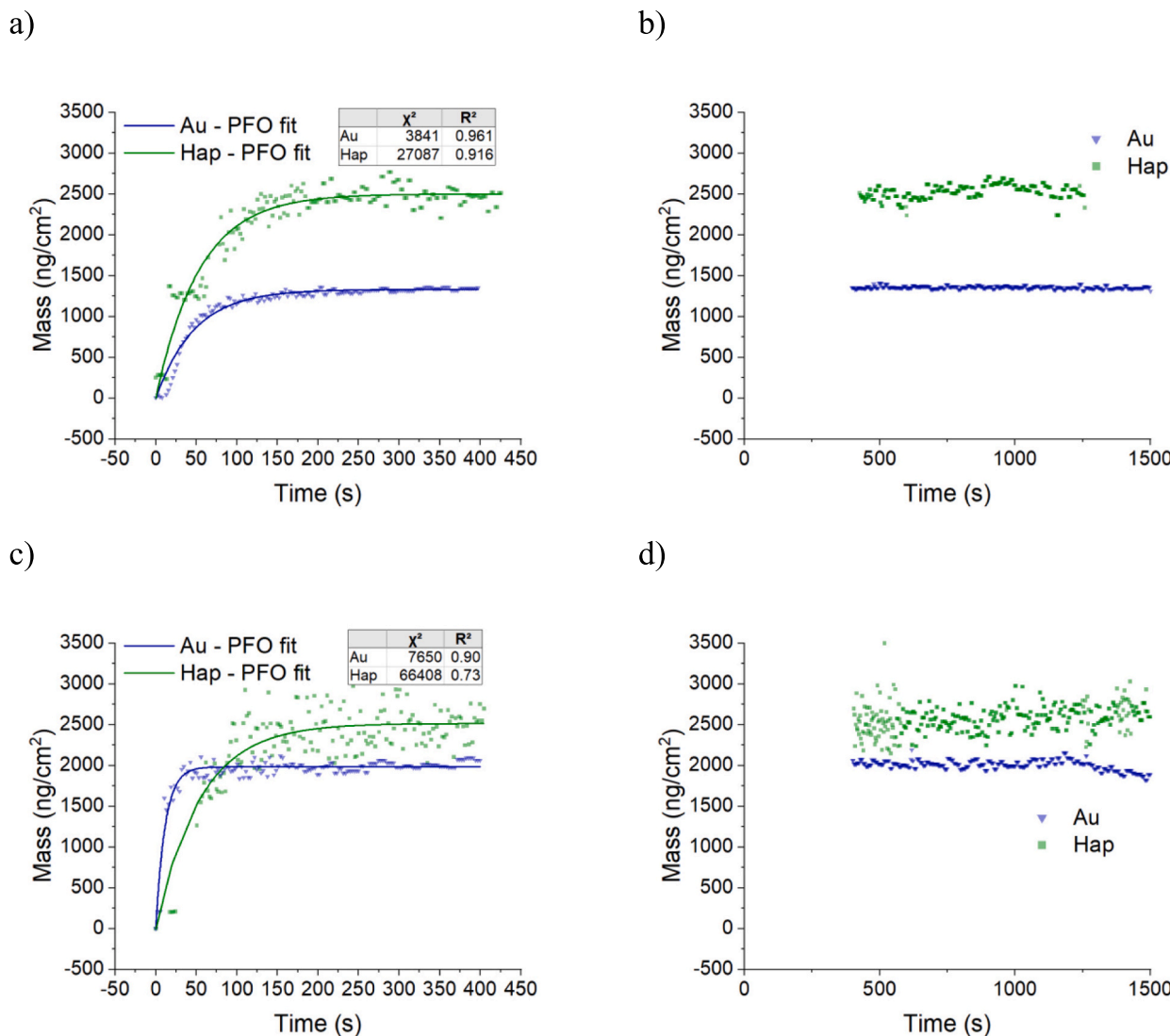


Fig. 5. Best fits of kinetic models for adsorption onto gold and hydroxyapatite for the first stage of layer growth of a) purified PGM and c) purified PGM + PBS, and second stage behaviour of b) purified PGM layers and d) purified PGM + PBS layers. (For interpretation of the references to colour in this figure legend, the reader is referred to the web version of this article.)

Table 1

Calculated fitting parameters of model growth of mucin layers on gold and hydroxyapatite surfaces. For PFO model, refer to k_1 and q_e , for PSO model k_2 and q_e , and for Elovich model, refer to α and β .

			As received			Purified			
	Solution	Material	Model	$k_1 / k_2 / \alpha$	q_e / β	Model	$k_1 / k_2 / \alpha$	q_e / β	
Initial 450 s	PGM	Au	Elovich	1.41E+03	2.41E-03	PFO	0.021	1332	
		Hap	PFO	0.013	2347	PFO	0.019	2500	
		Hap P1	Elovich	1.19E+02	7.39E-03	-	-	-	
		Hap P2	PFO	0.017	2256	-	-	-	
		PGM + PBS	Au	PSO	1.31E-04	1631	PFO	0.087	1984
Post 450 s	PGM + PBS	Hap	Elovich	1.51E+05	7.12E-03	PFO	0.018	2516	
		Solution	Material	Model	$k_1 / k_2 / \alpha$	q_e / β	Model	$k_1 / k_2 / \alpha$	q_e / β
		PGM	Au	Desorption	4.82E-05	3204	-	-	-
		Hap	Elovich	8.12E+02	3.00E-03	-	-	-	
		Hap	Elovich	8.23E+03	5.36E-03	-	-	-	

heterogeneous surfaces in addition to a chemisorption dominant adsorption pathway [63]. The PSO model for mucin adsorption onto gold also had a good fit, $R^2 < 0.89$, which was better than the PFO model, $R^2 < 0.71$. Furthermore, the calculated mass at equilibrium from

the PSO model, $q_e = 3077 \text{ ng/cm}^2$, was closer to the experimental mass value, 2973 ng/cm^2 compared to the PFO estimate, $q_e = 2850 \text{ ng/cm}^2$. While adsorption pathways can occur concurrently, the Elovich and PSO suggest that the dominant mechanism for adsorption may be via

chemisorption onto gold surfaces, potentially through strong electrostatic interactions or electron sharing. After a mass plateau was reached from PGM adsorption, a desorption stage occurred on the surface whereby mass was gradually lost from the surface as shown in Fig. 4 b). This suggested structural transformation within the mucin layer, attributed to the as received PGM solution alone.

The addition of perturbing PBS salts to the as-received mucin changed the adsorption model to follow the PSO model, with $R^2 < 0.90$ and $\chi^2 = 3404$. Furthermore, PGM + PBS enhanced the rate of mucin adsorption with less adsorbed mass at equilibrium, of 1631 ng/cm^2 . Once equilibrium was reached, no additional adsorption or desorption occurred as shown in Fig. 4 c) and d). This suggested that the presence of salts increased the protein layer formation rate, limited mucin layer adsorption, and promoted layer retention onto gold as no desorption was observed.

Purification of PGM also influenced adsorption behaviour to gold, as both purified PGM (pPGM) and purified PGM with additional PBS (pPGM + PBS) closely follow the PFO adsorption model, with $R^2 > 0.96$ shown in Fig. 5 a) and $R^2 = 0.90$ shown in Fig. 5 c) respectively. Rather than chemisorption dominating adsorption, physisorption was favoured under these conditions, which suggested the removal of key adsorption components from the as-received PGM solution during the purification process. On the one hand this is supported by the reduction in mass adsorbed onto gold (1332 ng/cm^2) under pPGM conditions. On the other hand, more mass was adsorbed onto gold (1984 ng/cm^2) under pPGM + PBS conditions compared to growth under pPGM and PGM + PBS conditions. Furthermore, the purified PGM solutions presented no additional adsorption or desorption once equilibrium was reached, shown in Fig. 5 b) and Fig. 5 d). This suggested 2 things, firstly a cooperation between PBS salts and molecules within the purified PGM solution promoted mucin layer formation, and secondly, layer retention onto gold because of PGM purification and/or additional PBS salts.

Data from kinetic adsorption models suggested that chemisorption dominant pathways were mostly attributed to layer adsorptions onto gold with PSO and Elovich model fits without purification. In the literature there are numerous adsorption pathways for salivary protein to gold as studied by QCM-D and ellipsometry alike, both via physisorption and chemisorption [16–20,26]. Salivary proteins have been shown to adsorb via electrostatic and hydrophobic interactions [16,17,45,61,65]. However, the term ‘electrostatic interactions’ is used broadly and does not specifically state the bonding strength associated with this type of adsorption. It may be assumed that the references to electrostatic interactions relates to the strong ionic interactions associated with chemisorption. It can therefore be inferred that the PSO and Elovich fits for mucin adsorption to gold supports the current understanding of adsorption.

Gold has been previously suggested to demonstrate mirror charge properties, presenting potential sites with opposing charges to charged molecules presented to the surface when following the electrostatic model of image charges [16,17]. This enables strong electrostatic adsorption during the initial growth phase of mucin onto gold, given presence of positive and negative sites on mucin from amine groups and sialic acid groups within carbohydrate chains respectively [34,57,61]. Furthermore, native mucin tends to possess cysteine regions and associated thiol groups which are known to facilitate strong covalent bonding onto gold surfaces via S–Au bonds [16–18,66,67]. This adsorption process has been shown to have an impact on increasing the mass adsorbed onto the surfaces of gold and increase a protein layer’s resistance to elution [16–18]. However, in commercial PGM (type II) the presence of cysteine groups has been observed to be absent, due to damage in the terminal regions from industrial purification processing [54]. While cysteines are lacking within type II PGM, remnants may still exist within the peptide terminals and glycol regions to facilitate thiol-gold bonding, but to a lesser degree compared to other pathways. While demonstrating a loss in commercial PGM functionality [54], it is unclear how the additional purification step used altered the protein

composition of type II PGM outside of removing protein contaminants. However, the current work suggests mucin-impurity interactions influence the adsorption pathway and layer’s structural conformation during adsorption onto gold. The removal of impurities in type II PGM, and the absence of functional mucin terminals mean that subsequent adsorption of purified PGM can only adsorb through physisorption pathways.

Surface interactions subsequently influence the structural behaviour and viscoelastic properties of the mucin layer on gold. A combination of strong/weak electrostatic interactions, hydrophobic/hydrophilic interactions and hydrogen bonding between mucins can promote a mucin network which determines the layer’s viscoelasticity [68]. When considering the second growth phase of as received PGM layer on gold after 450 s (Fig. 4 b)) desorption occurred, suggesting a structural transformation. Layers adsorbed onto gold by covalent bonding remain in a fixed orientation at the surface and are more resistant to elution by the continuously flowing mucin solution compared to non-thiolated proteins [67]. Proteins adsorbed by strong electrostatic interactions possess more freedom, switching between positive and negative mirror charges on the gold surface, desorbing and reabsorbing, permitting rotational and lateral movements [26]. The movement and subsequent desorption of free mucin from the surface may free up surface sites to which three things may occur. Firstly, this could be replaced by another mucin via strong electrostatic interactions. Secondly, this active site may drive chemisorption of mucin-impurities as a stronger S–Au bond can appropriate this location. Thirdly and finally, this site could remain unused because of the negative electrostatic repulsion of surrounding adsorbed mucin. In this system, over time the mass observed would reduce as cumulatively less mucin-impurities would be strongly bound to the gold surface.

In the present study the desorption from gold during the growth phase may be attributed to conformational changes of mucin at the surface in such a way that prevents subsequent adsorption to the surface, which has been observed with salivary pellicle growth [60]. On the other hand, Barrantes et al. [16] carried out similar experiments for saliva adsorption onto different surfaces using a QCM for a similar growth duration and no desorption was observed. The differences observed may be attributed to the more complex solutions (saliva) used for these experiments compared to the relatively simple industrially processed crude mucin (PGM) solution used in the current study. Other work has used more complex solutions such as pooled human saliva or an isolated protein which is subsequently mixed with a (PBS) solution [16,18,19,60,68]. It was suggested that the presence of an ionic component in the bulk solution or additional protein/polymer may be required to prevent mucin desorption from the surface and maintain ongoing adsorption [40]. The addition of PBS and separate purification of PGM prevented desorption in other tests, through either a reduction in interruption impurities within the solution or PBS salt interactions improving the stability of adsorbed layers.

3.2.2. Adsorption onto Hydroxyapatite Surfaces

Different adsorption kinetics were observed onto hydroxyapatite (Hap). Initial as received PGM adsorption, shown in Fig. 4 a), was best described by the PFO model, $R^2 < 0.92$ and $\chi^2 = 2858$. However, after 450 s the Elovich model provided a closer fit, $R^2 < 0.92$ and $\chi^2 = 2834$, shown in Fig. 4 b). Furthermore, the first stages of initial growth are split into two distinct adsorption curves, which follow an Elovich fit for the first 60 s, $R^2 < 0.97$ and $\chi^2 = 625$, followed by a PFO fit up to 450 s, $R^2 < 0.78$ and $\chi^2 = 1455$. This indicated that during the growth phase, adsorption onto the hydroxyapatite surface was mostly dominated by the physical adsorption of mucin onto the surface.

Like PGM adsorption onto gold, the addition of PBS salts increased the rate of adsorption onto hydroxyapatite whilst reducing the overall adsorbed mass compared to PGM only adsorption to hydroxyapatite, 1891 ng/cm^2 compared to 2347 ng/cm^2 . Unlike PGM + PBS adsorption to gold, the PFO kinetic model was preferred for adsorption onto hydroxyapatite, $R^2 < 0.92$ and $\chi^2 = 9068$, shown in Fig. 4 c). Similar to

PGM adsorption to hydroxyapatite after 450 s, adsorption continued following the Elovich model, $R^2 < 0.82$ and $\chi^2 = 1261$, shown in Fig. 4 d).

Purification of PGM presented no changes to the kinetic adsorption model for both pPGM and pPGM + PBS layer formation on hydroxyapatite. Both followed the PFO model, with $R^2 < 0.92$ and $R^2 < 0.73$ shown in Fig. 5 a) and c) respectively. The addition of PBS salts were shown to not influence purified PGM adsorption, which presented a similar adsorption rate and adsorbed mass to pPGM layers on hydroxyapatite, of 2516 ng/cm^2 compared to 2500 ng/cm^2 . This indicated that purified PGM interactions with PBS salts were negligible regarding hydroxyapatite adsorption. Therefore, differences between purified and as received PGM adsorption onto hydroxyapatite were attributed to layer conformation differences caused by the removal of solution impurities through purification. Furthermore, after 450 s, no additional adsorption or desorption occurred after mass adsorption equilibrium onto hydroxyapatite, shown in Fig. 5 b) and d). This behaviour further suggested the purification process had removed impurities from the as received PGM which influence later stage layer adsorption.

Mucin possesses a net negative charge from sialic acid groups and sulphates which are present in the central brush like region of their own carbohydrate chains, which in turn renders this structural region of mucin hydrophilic [34,57,61]. Hydrophobic regions exist on either side of the brush like region, to which there are many cysteine residues allowing disulphide bridging between other mucin monomers [34,57,61]. Finally, as with all amino acids, an amine group and carboxylic acid group exist in the structure of the mucin monomer. All these groups contribute to the complexity of mucin in terms of how it interacts with a surface or one another in each environment. Hydroxyapatite surfaces possess a net negative charge, like mucin, and localised surface charges determined by the exposure of the hydroxyapatite crystal structure [69]. Calcium regions are present on 'ac' and 'bc' crystal faces which impart a positive charge in solution, while phosphate regions on 'ab' faces impart a negative charge [69]. Depending on the oral environmental conditions, mucin therefore has multiple pathways to adsorb onto the uniform, crystalline hydroxyapatite surface of the Hap QCM-D sensors. Furthermore, should mucin adsorb onto calcium regions via sialic acid or carboxylic acid groups (negatively charged groups to positively charged sites), there is also the chance of cooperative binding taking place with additional hydrogen bonding between the amine groups and the phosphate regions [70,71].

Initial adsorption of the as received PGM was thought to be a result of negatively charged sialic acid groups on proteins initially binding to positively charged surface calcium regions, after which H bonding may then permit coordinate bonding with other locations [71]. This is supported in the current study by the rapid adsorption in Hap P1 which showed a stronger fit with Elovich model. The adsorption at this stage is more likely to be chemisorption driven whereby calcium sites are taken up by strong electrostatic interactions. This is followed by a stronger PFO fit during the Hap P2 stage which may be attributed to a combination of coordinate bonds forming with additional H bonding and hydrophobic interactions occurring concurrently. However, given the level of model fit for Hap 2, this may not be an adequate fit. Furthermore, with the absence of functional mucin terminals, mucin is less likely to adsorb via hydrophobic interactions [54], suggesting a larger dependence on surface ion interactions and H bonding. The addition of PBS salts was shown to disrupt any physisorption, with cation interactions potentially shielding phosphate regions thus reducing H bonding, as well as altering the mucin conformation, demonstrated by the Elovich adsorption fit. The applications of kinetic adsorption models alone cannot be used to determine the exact pathways for adsorption. While they are useful to describe how adsorption may be occurring, additional data that measures the energy changes during adsorption would be helpful in highlighting the type of adsorption occurring. This may help in future investigations to further differentiate the mechanistic pathways for mucin adsorption.

3.3. Friction Analysis of Mucin Layers on QCM Sensors

Tribo-tests were performed on QCM-D sensors to assess mucin solution lubrication on gold and hydroxyapatite surfaces to provide an indirect link to the modelled QCM-D properties. Fig. 6 shows the resultant frictional force response to incremental normal loading for all test solutions on gold and hydroxyapatite. A linear F_t response was observed over the varying load conditions, as has been observed for mucin previously [59]. Error bars represent the standard deviation about the mean tangential force for all samples ($n = 3$) at each normal load, while the mean dynamic coefficient of friction (μ) and standard deviation about μ was calculated from the linear F_t vs F_n curve fits of each sample in OriginLab (OriginLab Corp, USA). t -tests assessed significance for each interaction.

PGM adsorption improved lubricity of the Hap surface with a reduction in the coefficient of friction (μ) from 0.79 ± 0.03 in DiW to 0.24 ± 0.04 ($p < 0.001$). Interestingly, the gold surface's coefficient of friction increased with the adsorbed mucin layer from 0.42 ± 0.03 in DiW to 0.51 ± 0.02 in PGM, but this was not observed to be significant ($p = 0.990$). In PGM + PBS, the coefficient of friction reduced on both surfaces, from 0.51 ± 0.04 to 0.40 ± 0.03 on gold ($p = 0.980$), and from 0.75 ± 0.02 to 0.25 ± 0.02 on Hap ($p = 0.010$). The additional purification step was shown to influence the friction behaviour on both materials. The coefficient of friction with pPGM on gold and hydroxyapatite was greater compared to tribology tests with the crude PGM solutions, with $\mu = 0.57 \pm 0.02$ ($p = 0.823$) and $\mu = 0.38 \pm 0.01$ ($p = 0.980$), respectively, but not significantly. When compared with DiW alone, pPGM still improved lubrication on Hap significantly ($p < 0.001$). Interactions between pPGM and PBS salts had a limited effect on reducing the coefficient of friction on gold compared to PBS alone ($p = 0.999$), of $\mu = 0.40 \pm 0.02$, which was also comparable to PGM + PBS ($p = 0.999$). An interesting behaviour was observed with pPGM + PBS on Hap, where the F_t and F_n relationship was not linear over the loading range. When split, a higher coefficient of friction was observed between $F_n = 0.05\text{--}0.30 \text{ mN}$ of $\mu_1 = 0.79 \pm 0.04$, which reduced to $\mu_2 = 0.21 \pm 0.06$ between $F_n = 0.30\text{--}0.50 \text{ mN}$ ($p = 0.026$). The initial stage, μ_1 was comparable to PBS on Hap ($p = 0.948$), while μ_2 was comparable with PGM + PBS on Hap ($p = 0.725$).

All Hap surfaces presented differences when compared to gold surfaces under each condition. Coefficient of friction was greater on Hap surfaces without PGM and lower on Hap surfaces with PGM or pPGM. The differences in coefficient of friction between Hap and gold were observed to be significant under DiW ($p < 0.001$), and PBS conditions ($p = 0.050$). Significance was not observed between Hap and gold surfaces for PGM + DiW ($p = 0.305$), or PGM + PBS ($p = 0.690$) conditions. The presence of perturbing salts (PBS) was shown to have no influence on the coefficient of friction, for both a PBS only solution compared to DiW on gold and Hap ($p = 0.882$ and $p = 0.999$ respectively), for PGM + PBS compared to PGM + DiW on gold and Hap ($p = 0.999$ and $p = 0.999$ respectively), and for pPGM + PBS compared to pPGM + DiW on gold ($p = 0.931$). However, both μ_1 and μ_2 of pPGM + PBS indicated PBS salts had an influence on the purified PGM interactions with Hap compared with pPGM + DiW ($\mu_1 - p = 0.014$ and $\mu_2 - p = 0.074$).

Overall, these results suggest that the surface material interactions with crude PGM have a greater influence on resultant lubrication. This is independent of additional PBS salts which presented little change to the coefficient of friction compared non-PBS solutions. PGM interactions with Hap surfaces demonstrated the importance of protein solution-surface interactions in promoting enhanced lubrication, and that changing the composition of PGM through purification also changes the sensitivity to these surface specific interactions.

3.4. Linking Tribology with Structure

The term "structural softness" has been used previously in the literature to provide a qualitative assessment of soft bio-polymer layers and

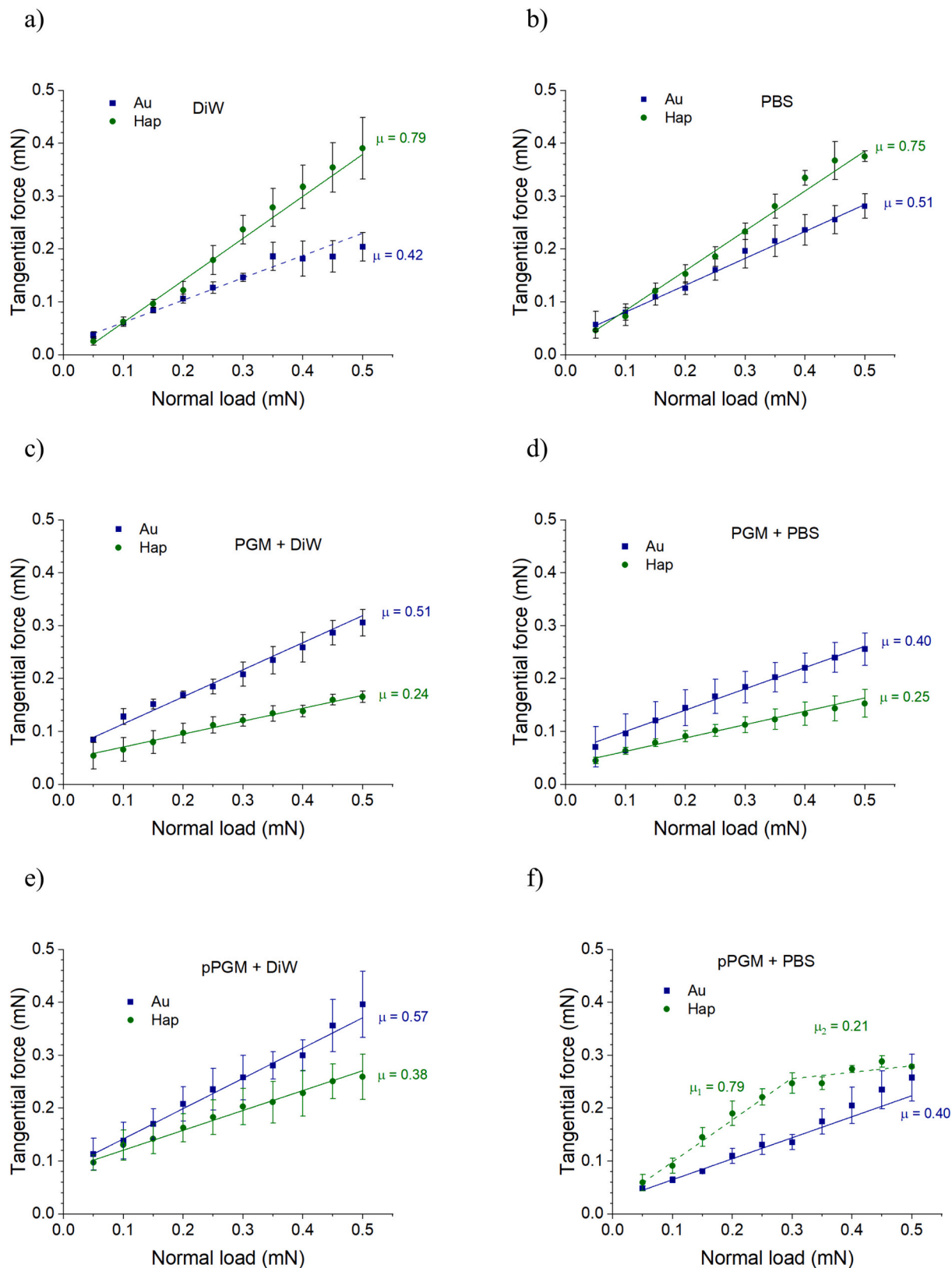


Fig. 6. Mean tangential force from gold and hydroxyapatite QCM sensors over incremental normal load with a) DiW, b) PBS, c) PGM + DiW, d) PGM + PBS, e) pPGM + DiW and f) pPGM + PBS. (For interpretation of the references to colour in this figure legend, the reader is referred to the web version of this article.)

their structure, defined as the ratio of the layer's dissipation, ΔD , over change in frequency, Δf , for a given overtone [33]. Physically this ratio is a measure of the energy lost due to the dampening effect of the layer per unit mass change, combining both shear elasticity and viscosity terms [42,73]. The mean structural softness of the PGM layer on gold was calculated 0.43 ± 0.08 at equilibrium, which has been shown in Fig. 3 to be a softer and dissipative layer. For hydroxyapatite, the structural softness for PGM layers were comparable to those observed for whole saliva on the same surface in another study, Veeregowda et al. [33], between 0.16 and 0.26. Building on this qualitative measure, it was hypothesised that the calculated layer thickness, viscosity and shear modulus values may also provide additional insight to the overall lubrication. To investigate any potential links between the structural properties of different PGM layers and the observed coefficient of friction, linear and non-linear regression analyses were performed on each separate material, shown in Fig. 7 and Fig. 8 for gold and hydroxyapatite surfaces respectively. Most trends were fitted using a linear fit, which presented an optimal R^2 value, except for the shear modulus property on hydroxyapatite which was fitted with a non-linear fit.

On gold no strong trends were observed between the coefficient of friction and structural softness, thickness and viscosity properties of the layer. However, an interesting trend was observed with an increased coefficient of friction and with the layer's shear modulus property on gold $R^2 > 0.68$, shown in Fig. 7d). On hydroxyapatite, trends were observed with a reduced coefficient of friction with increasing layer properties, with stronger trends between the coefficient of friction and viscosity, thickness and shear modulus properties with fits of $R^2 = 0.66$, $R^2 > 0.77$ and $R^2 > 0.96$ respectively. These results suggest that for hydroxyapatite surfaces the viscosity and shear modulus of the PGM layers, shown in Fig. 8c) and d), play a role in reducing the coefficient of

friction. This could be dependent on the viscoelasticity of the interfacial lubricating layer in addition to plastic deformation on the surface [74].

3.4.1. Importance of Structural Property Measurements

In the absence of structural proteins, both water and ionic (PBS) solutions alone are unable to bear the load of high-pressure contacts sliding over each other at low sliding speeds, as used in the current experimental work. This can result in direct boundary contact between interacting surfaces which will generate larger coefficients of friction, as observed for the Hap surface in Fig. 6a) and b). When considering salivary films, the bio-lubrication has been hypothesised to link to two characteristics, the structure of the adsorbed layer and the degree of glycosylation of the proteins within the structure [33]. Given that the same type and batch of PGM was used in all growth solutions, the degree of glycosylation can be assumed to be similar for the sake of comparison between crude solutions in water and PBS environments, and between purified solutions in the same environment separately. The additional purification step would have reduced the overall degree of glycosylation, resulting in a less functional PGM solution that impacted lubrication [54], which was observed on hydroxyapatite surfaces in Fig. 6, however this had little effect on gold surfaces. Nevertheless, a structural network is required to trap water molecules within its structure at the liquid surface interface and effectively provide viscous lubrication during sliding conditions [40].

PGM has been previously shown to reduce the coefficient of friction compared to that of deionised water on bovine enamel surfaces [27]. As Hap is the main component of tooth enamel, it is no surprise that this reduction in tangential force and coefficient of friction occurs in the current study. Additionally, PGM has been shown to reduce the coefficient of friction the gold surfaces under similar operating conditions

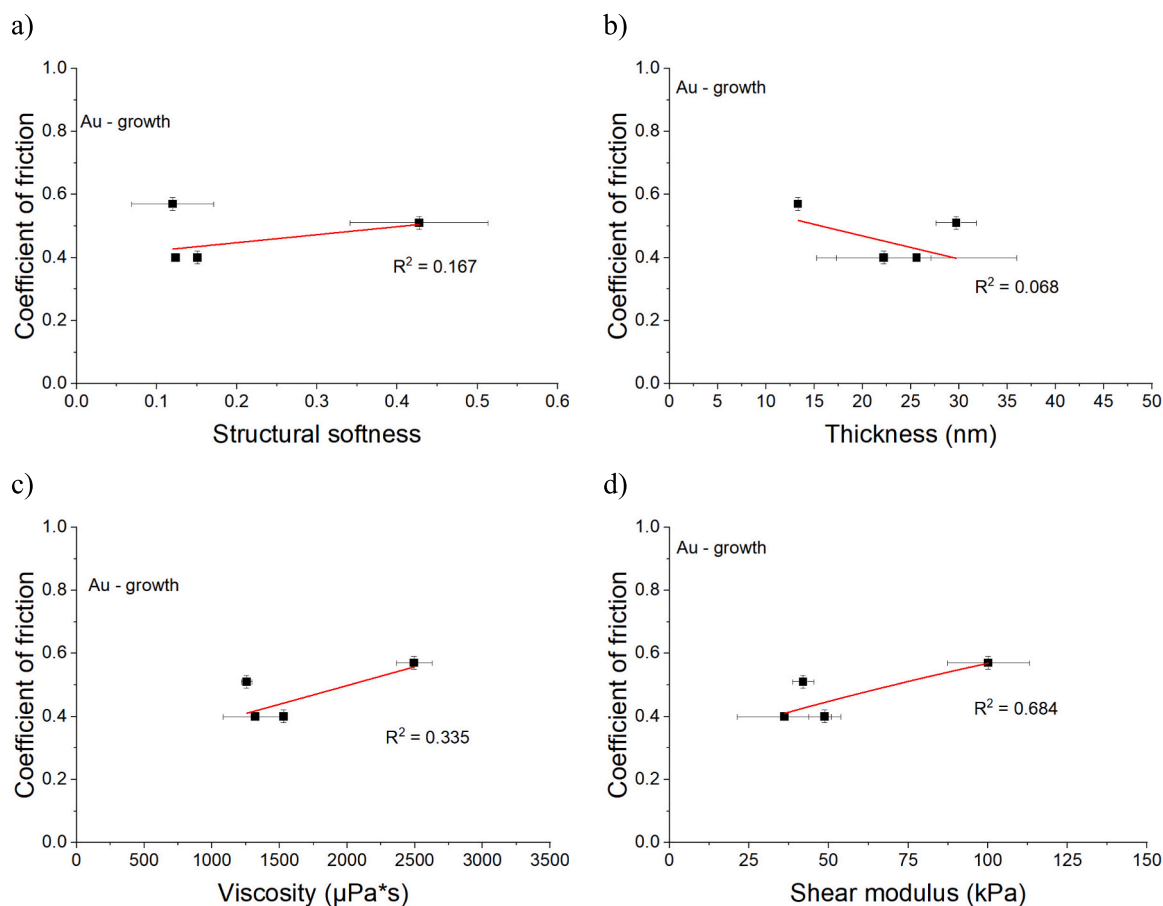


Fig. 7. Regression analysis comparing the measured coefficient of friction with a) structural softness, b) thickness, c) viscosity and d) shear modulus on gold. (For interpretation of the references to colour in this figure legend, the reader is referred to the web version of this article.)

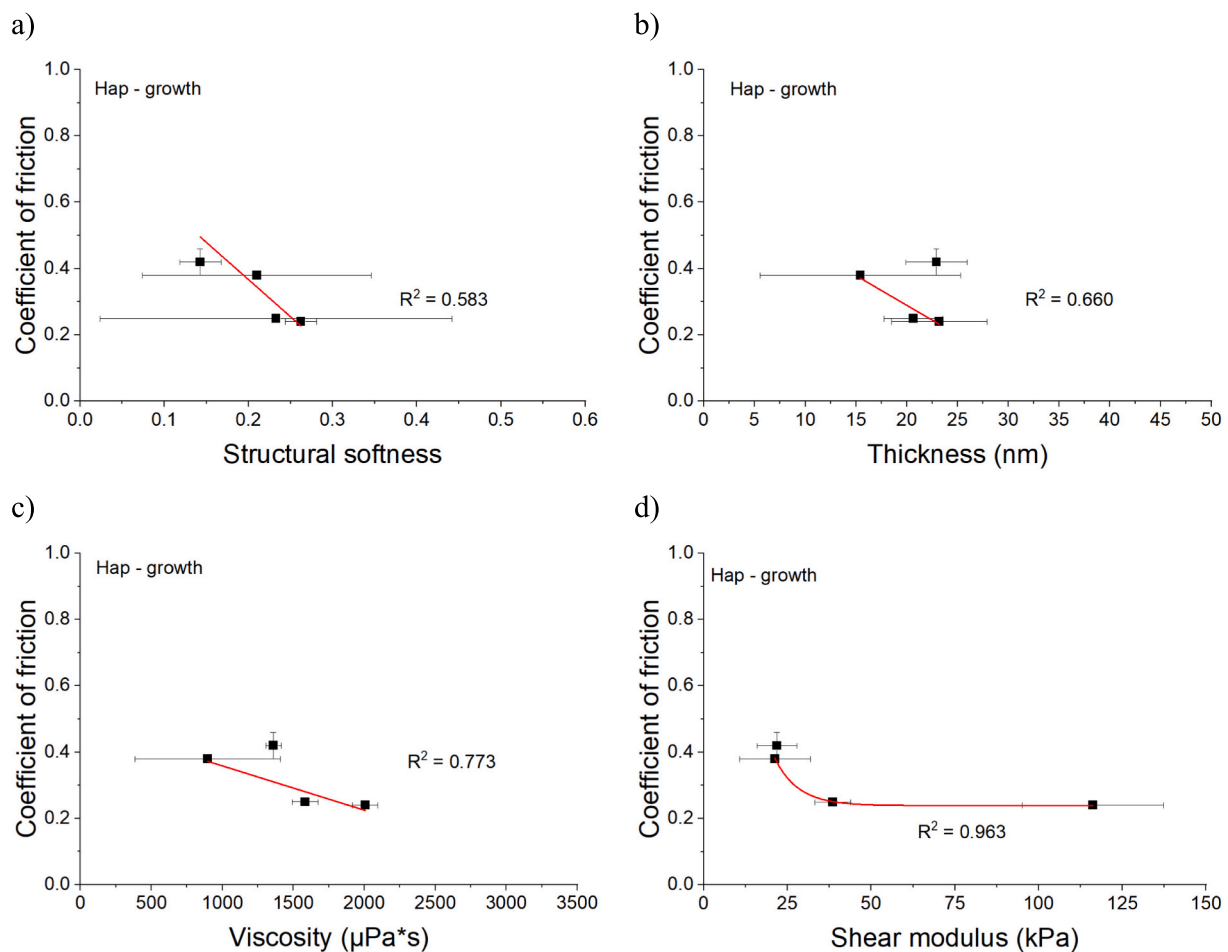


Fig. 8. Regression analysis comparing the measured coefficient of friction with a) structural softness, b) thickness, c) viscosity and d) shear modulus on hydroxyapatite.

[72]. The entrapment of water within a mucin network at the surface may therefore shift the shear plane away from the surface, adopting a hydration lubrication regime similar to hydrogels. Friction behaviour of polymer hydrogels has also been observed to be influenced by elastic deformation and viscous damping components [82]. Lubrication in water was shown to increase the viscous component of friction compared with air, and reduced the elastic deformation component of friction which reduced the overall friction force [82]. The elastic deformation of the layer was important in terms of overall friction.

The viscoelasticity of salivary layers depends upon the mucin component to trap water molecules within the structure of the pellicle, as has been shown when comparing parotid and whole human saliva [33,52,60]. The structural softness on hydroxyapatite in the current study is outside of the range previously observed for saliva [33] and will be attributed to the additional mucin interactions with other salivary proteins that may modify the layer's structure to be more rigid [78]. Similar values were observed for bovine submaxillary mucin to PDMS in different salt concentrations, between 0.20 and 0.25 [40]. The reduced competition between proteins and ions enables a more spread-out mucin structure which will impact load bearing capacity, viscous lubrication, charge density and osmotic pressure between a sliding contact [59,74,79]. Veeregowda et al. [33] suggested that a higher structural softness and increased hydrophilicity of a protein layer might improve bio-lubrication, when examined with atomic force microscopy, which supports the trends observed for structural softness on hydroxyapatite shown in Fig. 8a), with $R^2 > 0.58$.

Furthermore, changes to structural softness were observed in studies

which modified preformed salivary films to assess the relief of dry mouth for Xerostomia patients [80,81]. Increased structural softness was shown to improve lubrication under colloidal probe atomic force microscopy, however under a tongue-enamel friction system no changes to the coefficient of friction were observed [81]. Under the tongue-enamel system, increased structural softness was linked to a longer dry mouth relief period rather than an overall reduction in the coefficient of friction [80]. This highlights the complexity of linking friction behaviour between the nanoscale and macroscale, and through a single measure of the layer's structural composition.

3.4.2. The Effect of PGM Purification

The additional purification process used in this work is known to remove molecules smaller than the dialysis cut-off (100 kDa), which relates to impurities from DNA, mucin fragments, cellular debris, salts and smaller proteoglycans [57,76]. The resultant solution was one which contained a more dysfunctional PGM molecules which have been described to lack functional terminal groups and sialic acid groups compared to natively acquired PGM and other commercial PGM (type III) after purification [54]. This significantly impacted the structure of layers grown on gold and hydroxyapatite, producing a thinner layer with different viscoelastic properties. On gold, a higher shear modulus and viscosity was observed which were structurally similar to crude PGM layers on hydroxyapatite whilst presenting a higher coefficient of friction. Similarly, purified PGM layers on hydroxyapatite presented a higher coefficient of friction compared to crude PGM layers but with a much lower layer viscosity and shear modulus. Changes to the friction

behaviour of mucin because of purification has been observed before with a different type of commercially available mucin. BSM lubrication was examined between PDMS tribopairs, for crude, dialysis purified and anion exchange chromatography filtered BSM, to find that both purified variants outperformed the as received mucin by reducing the coefficient of friction [62]. Lubrication from the crude mucin was said to be dominated by non-slippery, lighter and larger molecules in the contact area, where the presence of bovine serum albumin in BSM layers presented stiffer and more viscous films responsible for higher friction [62]. From a layer property perspective, this supports what is observed for purified PGM layers on gold, but not the more hydrophilic hydroxyapatite surface. Lubrication was proposed to be improved between hydrophobic tribo-contact through BSM suppressing adhesion action, especially under low contact pressures and high surface compliance [62]. In contrast the current work examines high contact pressures and low compliance tribo-pairs, between hydrophilic Y-TZP and gold/hydroxyapatite surfaces where different layer structures and lubrication were expected. The reduced lubrication from PGM and pPGM layers on gold might be therefore be attributed the layer's structural conformation increasing adhesion forces between itself and opposing structures on the opposing surface, although this cannot be confirmed as the Y-TZP surface was not investigated. The opposite was observed on hydroxyapatite surfaces.

3.4.3. The Role of Added Salt Interactions

On gold surfaces, PBS salts had little effect on the layer structure. The PGM + PBS layer's shear modulus and viscosity properties were close to PGM + DiW layer properties, whilst decreasing layer thickness. This behaviour suggested that the combined salt solution did not have much of an impact on improving lubrication on gold. The addition of PBS to PGM had no beneficial effect of hydroxyapatite lubrication, presenting a similar coefficient of friction value compared to PGM + DiW. A reduced shear modulus, viscosity and layer thickness suggested salt disruption within the layer itself, potentially by competing with contact sites on the surface or by preventing intermolecular crosslinking [77]. This friction behaviour was also observed for a Y-TZP and bovine enamel tribopair in previous work by the current author, with little improvement to lubrication with PGM + PBS compared to the base PGM solution [27]. It was thought the addition of PBS provided a surface fortification benefit and additional wear resistance under sliding conditions. The purification of PGM with PBS presented no change to lubrication on gold, with similar layer properties to unpurified PGM with PBS. Interestingly, a high coefficient of friction on hydroxyapatite under pPGM + PBS was observed under low loading conditions which was comparable to PBS without additional protein component, which was subsequently followed by a relatively low coefficient of friction under higher loading [74].

3.4.4. The Role of the Adsorption Pathway on Layer Structure and Lubrication

The chemisorption and subsequent desorption of the mucin layer suggested layer conformation changes occurred during the formation of the PGM layer on gold, as shown in Fig. 3 and Fig. 4, suggesting a layer that favoured thiol bonded mucin/ mucin fragments or strongly bound impurities. This is shown by the reduced shear moduli in Fig. 2, indicating less interaction within the mucin layer. Under these conditions it might be thought that an untangled layer structure might be considered for the gold surface, with a combination of upright and horizontal PGM molecules and PGM/impurity aggregates on the surface, as indicated in the schematic presented in Fig. 9a). While the carbohydrate chains within PGM can trap water to the structure, flow may still be permitted throughout the layer. When compressed under sliding, water is not fully trapped in the contact and may be squeezed out and the resultant shear plane being closer to boundary-boundary interactions [74]. Following these interactions, layer removal may occur over the tribological contact, to which components within the PGM solution may rapidly re-adsorb to the exposed areas [72,75]. The addition of salts builds into

the proposed structure when considering cations as hydration shells, integrating into the adsorbed mucin layer [74].

Conversely, the mucin layer on the Hap surface is thinner, but exhibits a larger shear viscosity and shear modulus properties. As mentioned earlier the adsorption is initially dominated by physisorption pathways with some degree of chemisorption. The more diverse bonding between PGM components and hydroxyapatite may permit a stronger layer network within the layer, forming a comparatively more rigid layer compared to what is formed on gold [40]. This is supported by a mean structural softness value of 0.24 ± 0.01 which was calculated at equilibrium towards the end of the growth stage. Furthermore, the significantly larger shear viscosity of the Hap mucin layer suggests that more water molecules are trapped in the layer's structure and are less free to flow. A "bridge" like mucin layer structure can be considered, trapping water between the mucin monomer and the surface, which is presented in Fig. 9b). This structure may also expose hydrophilic regions of mucin to the bulk fluid, permitting an extension to the hydration layer. Under sliding conditions, water flow is prevented from the layer which may move the shear plane further away from the surface [60]. Furthermore, hydration shells of unbound protein within the sliding contact may provide additional hydration repulsion between the mucin/Hap interface and the contacting body which in turn reduces the friction [74]. This effect may be less pronounced on the PGM/gold layer, which may explain the lack of lubrication observed for gold in the current study.

Purified PGM layers in Fig. 9c) and d) present different layer configurations accounting for the removal of impurities and the increased dysfunctionality of PGM to trap water molecules. These layers are thinner, lacking the bulk mass provided by impurities and PGM fragments, and present reduced lubrication under deionised water conditions. The addition of PBS ions partially serves to improve lubrication on gold, however their presences also disrupts PGM-surface interactions. This has a greater impact under purified conditions when considering the physisorption dominated adsorption of purified PGM onto both gold and hydroxyapatite.

Future work should aim to examine how these parameters change along with structural softness and how alternative polymers, proteins or ionic components alter this. Furthermore, the structural softness should be considered with additional parameters, such as layer hydrophilicity, to further understand the link with friction in future studies on specific material surfaces. Finally, follow up studies should investigate how mucin functionality and type influence adsorption and lubrication to gain further insight into the mechanism and impact of the initial stages of adsorption.

4. Limitations of Study

One of the limitations of this study relates to the use of Y-TZP as counter surface for tribological testing as this only focused on one type of material interrogation with PGM layers on gold and hydroxyapatite. The observed friction behaviour would be expected to be different using metallic or polymeric probes that might present different interaction between free and bound mucin in the tribological contact.

One other limitation was the sole use of commercial PGM type II, while other mucin sources exist for use within the field of oral and dental tribology. While this study demonstrated improved lubrication under certain conditions and an approach to assess potential links between lubrication and layer properties, it is limited by the use of a controversial mucin source. Additional work investigating native purified PGM and/or commercial BSM may build on this approach in the future.

5. Conclusion

The current study has shown differences in viscoelastic properties exist between mucin layers formed on gold and hydroxyapatite surfaces. Furthermore, these layers then go on to show differences in the observed

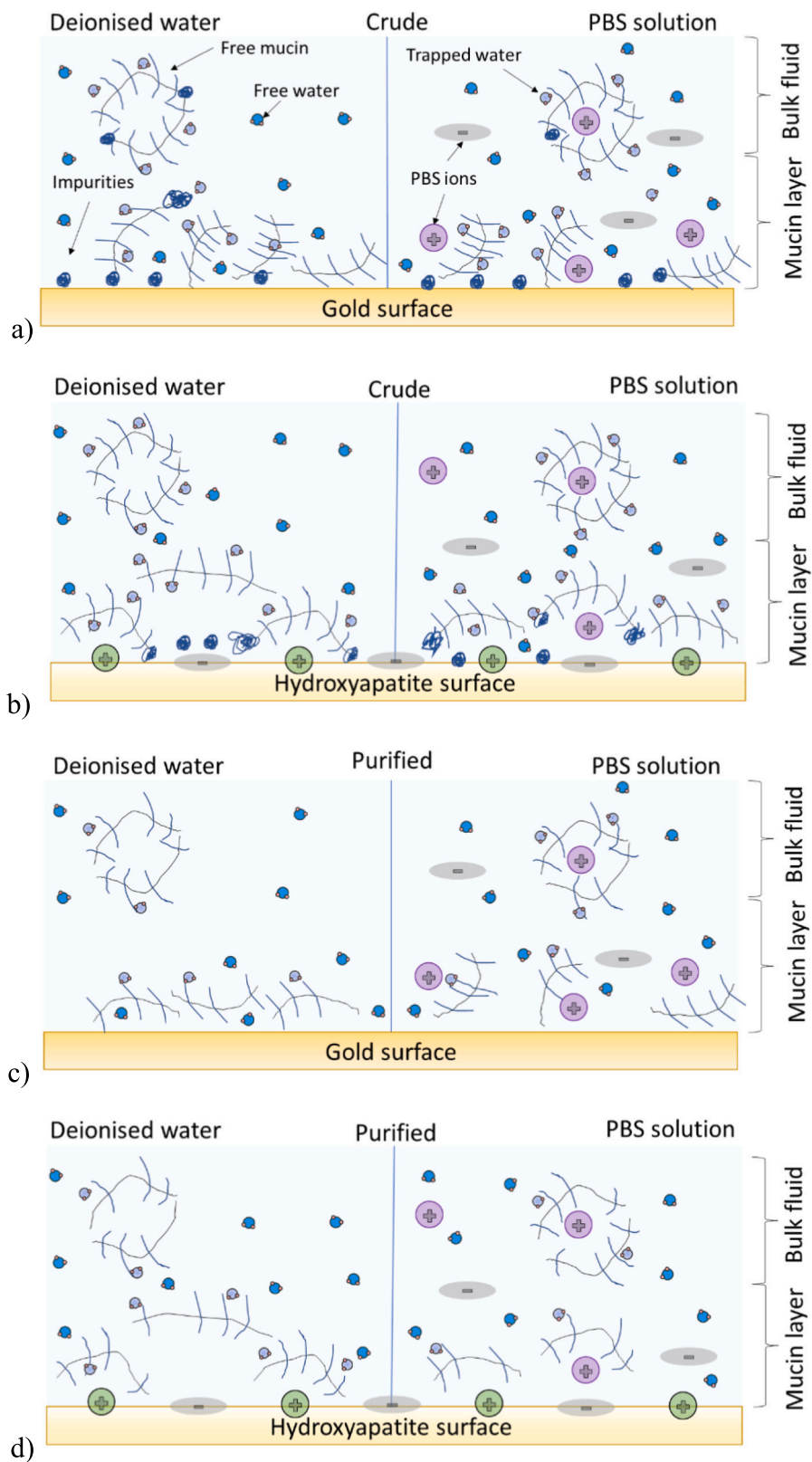


Fig. 9. Hypothesised crude PGM layers on a) gold and b) hydroxyapatite surfaces, and purified PGM layers on c) gold and d) hydroxyapatite surfaces prior to sliding. (For interpretation of the references to colour in this figure legend, the reader is referred to the web version of this article.)

friction behaviour, suggesting a potential link between layer formation and subsequent tribology. While it demonstrated that a higher structural softness ratio, $\Delta D/\Delta f$, would provide enhanced bio-lubrication on hydroxyapatite, data should also look closer at the viscosity and shear modulus properties of a layer in relation to tribological experiments. To alleviate the symptoms of xerostomia (dry mouth syndrome) and provide optimal oral protection and lubrication, further insights into potential therapies are needed. Following on from previous research to identify mucin's role on the tribocorrosion of dental tissues, this work assessed the adsorption behaviour of PGM on different dental surfaces. This included the growth and related properties of mucin layers, to gain insights into mucin's layer forming properties, and how it may link to oral lubrication. This work concludes that:

- PGM adsorption onto gold and hydroxyapatite is driven by surface interactions which are specific to the surface composition and may ultimately affect the resultant viscoelasticity of a fully formed PGM layer.
- The application of kinetic adsorption models in addition to $\Delta D/\Delta f$ plots provided additional insight into the potential adsorption sequence of mucins layers onto gold and hydroxyapatite surfaces. Stronger surface bonding is associated with mucin onto gold surfaces, while adsorption onto hydroxyapatite may be dominated by weaker physisorption mechanisms.
- Mucin layers formed on hydroxyapatite were shown to improve lubrication which may be linked to the layer's viscosity and shear modulus properties.
- Purification of commercial PGM had little impact on improving lubrication on hydroxyapatite and gold surfaces when compared to crude PGM.

Funding Sources

This work was supported by the Engineering and Physical Sciences Research Council (Award No. 1808962).

Declaration of Competing Interest

None.

Data availability

Data will be made available on request.

Acknowledgements

The authors would like to acknowledge the contribution of Professor Anne Neville for her expertise, support in conceptualisation, and guidance throughout most aspects of this study.

References

- [1] N.M.A. Chaudhury, P. Shirlaw, R. Pramanik, G.H. Carpenter, G.B. Protor, Changes in saliva rheological properties and mucin glycosylation in dry mouth, *J. Dent. Res.* 94 (12) (2015) 1660–1667.
- [2] B.A. Agostini, G.O. Cericato, E.R. Silveira, G.G. Nascimento, F. dos Santos Costa, W. M. Thomson, F. Demarco, How common is dry mouth? Systematic review and Meta-regression analysis of prevalence estimates, *Braz. Dent. J.* 29 (6) (2018) 606–618.
- [3] B. Liu, M.R. Dion, M.M. Jurasic, G. Gibson, J.A. Jones, Xerostomia and salivary hypofunction in vulnerable elders: prevalence and etiology, *Oral Med.* 114 (1) (2012) 52–60.
- [4] S.B. Jensen, A.M.L. Pedersen, A. Vissink, E. Andersen, C.G. Brown, C.G. Brown, A. N. Davies, J. Dutilh, J.S. Fulton, L. Jankovic, N.N.F. Lopes, A.L.S. Mello, L. V. Muniz, C.A. Murdoch-Kinch, R.G. Nair, J.J. Napenas, A. Nogueira-Rodrigues, D. Saunders, B. Stirling, I. von Bultzingslowen, D.S. Weikel, L.S. Elting, F.K. L. Spijkervet, M.T. Brennan, A systematic review of salivary gland hypofunction and xerostomia induced by cancer therapies: prevalence, severity and impact on quality of life, *Support Care Cancer* 18 (8) (2010) 1039–1060.
- [5] B. Malicka, U. Kaczmarek, K. Skoskiewicz-Malinowska, Prevalence of xerostomia and the salivary flow rate in diabetic patients, *Adv. Clin. Exp. Med.* 23 (2) (2014) 225–233.
- [6] J.M. Plemons, I. Al-Hashimi, C.L. Marek, Managing xerostomia and salivary gland hypofunction: executive summary of a report from the American dental association council on scientific affairs, *J. Am. Dent. Assoc.* 145 (8) (2014) 867–873.
- [7] U. Lendenmann, J. Grogan, F.G. Oppenheim, Saliva and dental pellicle: a review, *Adv. Dent. Res.* 14 (2000) 22–28.
- [8] I.C. Berg, M.W. Rutland, T. Arenbrant, Lubricating properties of the initial salivary pellicle – an afm study, *Biofouling* 19 (6) (2003) 365–369.
- [9] W.L. Siqueira, H.C. Margolis, E.J. Helmerhorst, F.M. Mendes, F.G. Oppenheim, Evidence of intact histatins in the in vitro acquired enamel pellicle, *J. Dent. Res.* 89 (2010) 626–630.
- [10] S.P. Humphrey, R.T. Williamson, A review of saliva: Normal composition, flow, and function, *J. Pros. Dent.* 85 (2) (2001) 162–169.
- [11] P.D.V. de Almeida, A.M.T. Gregio, M.A.N. Machado, A.A.S. de Lima, L.R. Azevedo, Saliva composition and functions: a comprehensive review, *J. Contemp. Dent. Pract.* 9 (3) (2008) 72–80.
- [12] M. Moritsuka, Y. Kitasako, M.F. Burrow, M. Ikeda, J. Tagami, S. Nomura, Quantitative assessment for stimulated saliva flow rate and buffering capacity in relation to different ages, *J. Dent.* 34 (9) (2006) 716–720.
- [13] J.B.D. Featherstone, Dental caries: a dynamic disease process, *Aus. Dent. J.* 53 (2008) 286–291.
- [14] A. Sarkar, E. Andablo-Reyes, M. Bryant, D. Dowson, A. Neville, Lubrication of soft oral surfaces, *Curr. Opin. Colloid Interface Sci.* 39 (2019) 61–75.
- [15] Y.F. Zhang, J. Zheng, L. Zheng, X.Y. Shi, L.M. Qian, Z.R. Zhou, Effect of adsorption time on the lubrication properties of the salivary pellicle on human tooth enamel, *Wear* 301 (1–2) (2013) 300–307.
- [16] A. Barrantes, T. Arnebrant, L. Lindh, Characteristics of saliva films adsorbed onto different dental materials studied by QCM-D, *Colloids Surf. A* 442 (2014) 56–62.
- [17] T. Halthur, T. Arnebrant, L. Macakova, A. Feiler, Sequential adsorption of bovine mucin and lactoperoxidase to various substrates studied with quartz crystal microbalance with dissipation, *Langmuir* 26 (7) (2010) 4901–4908.
- [18] E. Yoshida, T. Hayakawa, Adsorption study of pellicle proteins to gold, silica and titanium by quartz crystal microbalance method, *Dent. Mater. J.* 31 (6) (2013) 883–887.
- [19] M. Glumac, C. Ritzoulis, J. Chen, Surface properties of adsorbed salivary components at a solid hydrophobic surface using a quartz crystal microbalance with dissipation (QCM-D), *Food Hydrocoll.* 97 (105195) (2019) 1–8.
- [20] Q. Zeng, G. Ma, H. Xiao, D. Yang, L. Zheng, Z. Zhou, Effect of saliva flow rate on the adsorption kinetics and lubrication of salivary pellicle on human tooth enamel surface, *Wear* 426–427 (2019) 180–185.
- [21] K.C. Dee, D.A. Puleo, R. Bizios, Chapter 3: Protein-surface interactions, in: *An Introduction to Tissue-Biomaterial Interactions*, Wiley & Sons, inc, Hoboken, New Jersey, 2002, pp. 37–52.
- [22] M. Hannig, A. Joiner, The structure, function and properties of the acquired pellicle, *Monogr. Oral Sci.* 19 (2006) 29–64.
- [23] L. Lindh, I.E. Svendsen, M. Cardenas, T. Arnebrant, The salivary mucin MUC5B and lactoperoxidase can be used for layer-by-layer film formation, *J. Colloid Interface Sci.* 310 (1) (2007) 74–82.
- [24] P. Zhang, Y.P. Chen, W. Wang, Y. Shen, J.S. Guo, Surface plasmon resonance for water pollutant detection and water process analysis, *Trends Anal. Chem.* 85, no. C (2016) 153–165.
- [25] K. Haberska, O. Svenson, S. Shleev, L. Lindh, T. Arnebrant, T. Ruzgas, Activity of lactoperoxidase when adsorbed on protein layers, *Talanta* 76 (2008) 1159–1164.
- [26] I. Svendsen, L. Lindh, U. Elofsson, T. Arnebrant, Studies on the exchange of early pellicle proteins by mucin and whole saliva, *J. Colloid Interface Sci.* 321 (1) (2008) 52–59.
- [27] P. Smart, A. Neville, M. Bryant, Tribocorrosion of dental tissues: the role of mucin, *Tribol. Int.* 148 (2020) 1–8.
- [28] M.C. Jordao, F.Q. Ionta, B.T. Bergantin, G.C. Oliveira, M.J. Moretto, H.M. Honorio, T.C. Silva, D. Rios, The effect of mucin in artificial saliva on erosive rehardening and demineralization, *Caries Res.* 51 (2017) 136–140.
- [29] F.C. Ionta, F.L. Mendonca, G.C. Oliveira, A.R.B. Alencar, H.M. Honorio, A. C. Magalhaes, D. Rios, In vitro assessment of artificial saliva formulations on initial erosion remineralization, *J. Dent.* 42 (2014) 175–179.
- [30] M. Levine, Development of artificial salivas, *Crit. Rev. Oral Biol. Med.* 4 (3/4) (1993) 279–286.
- [31] B.G. Cooper, C. Bordeianu, A. Nazarian, B.D. Snyder, M.W. Grinstaff, Active agents, biomaterials, and technologies to improve biolubrication and strengthen soft tissues, *Biomaterials* 181 (2018) 210–226.
- [32] H. Teixeira, A.C. Branco, I. Rodrigues, D. Silva, S. Cardoso, R. Coloco, A.P. Serro, C. G. Figueiredo-Pina, Effect of albumin, urea, lysozyme and mucin on the triboactivity of Ti6Al4V/zirconia pair used in dental implants, *J. Mech. Behav. Biomed. Mater.* 118 (2021).
- [33] D.H. Veeregowda, H.J. Busscher, A. Vissink, D.-J. Jager, P. Sharma, H.C. Van der Mei, Role of structure and glycosylation of adsorbed protein films in biolubrication, *PLoS One* 7 (8) (2012) 1–10.
- [34] J.M. Coles, D.P. Chang, S. Zauscher, Molecular mechanisms of aqueous boundary lubrication by mucinous glycoproteins, *Curr. Opin. Colloid Interface Sci.* 15 (2010) 406–416.
- [35] J. Mystkowska, H. Car, J.R. Dabrowski, J. Romanowska, M. Klekotka, A. J. Milewska, Artificial mucin-based saliva preparations - physicochemical and Tribological properties, *Oral Health Prev. Dent.* 16 (2) (2018) 183–193.

- [36] C.E. Christersson, L. Lindh, T. Arnebrant, Film-forming properties and viscosities of saliva substitutes and human whole saliva, *Eur. J. Oral Sci.* 108 (5) (2000) 418–425.
- [37] A. Vissink, H.A. Waterman, E.J. Gravenmade, A.K. Panders, A. Vermeij, Rheological properties of saliva substitutes containing mucin, carboxymethylcellulose or polyethylenoxide, *J. Oral Pathol.* 13 (1984) 22–28.
- [38] A.T. Hara, C. Gonzalez-Cabezas, B.M. Sener, T. Attin, A. Weigand, The effect of human saliva substitutes in an erosion-abrasion cycling model, *Eur. J. Oral Sci.* 116 (2008) 552–556.
- [39] E. Andrysewicz, J. Mystkowska, J.R. Dabrowski, R. Olchowik, Influence of self-made saliva substitutes on tribological characteristics of human enamel, *Acta Bioeng. Biomech.* 16 (2) (2014) 67–74.
- [40] F. Xu, E. Liams, M. Bryant, A.F. Adedeji, E. Andablo-Reyes, M. Castronovo, R. Ettelaie, T.V.J. Charpentier, A. Sarkar, A self-assembled binary protein model explains high performance salivary lubrication from macro to nanoscale, *Adv. Mater. Interfaces* 7 (1901549) (2020) 1–17.
- [41] Guide: QCM-D data analysis - When to use Sauerbrey equation and when to use viscoelastic modelling, *Biolin Scientific*, 2022.
- [42] M.V. Voinova, M. Rodahl, M. Jonson, B. Kasemo, Viscoelastic acoustic response of layered polymer films at fluid-solid interfaces: continuum mechanics approach, *Phys. Scr.* 59 (5) (1999) 391–396.
- [43] W.P. Mason, R.N. Thurston, W. Philipoff, Relaxation in polymer solutions, liquids and gels, in: *Physical Acoustics: Principles and Methods*, Academic Press, New York, 1965.
- [44] X. Guo, J. Wang, A general kinetic model for adsorption: theoretical analysis and modelling, *J. Mol. Liq.* 288 (2019) 1–8.
- [45] M.A. Al-Ghuoti, D.A. Da'ana, Guidelines and interpretation of adsorption isotherms models: a review, *J. Hazard. Mater.* 493 (2020) 1–22.
- [46] Y.S. Ho, Review of second-order models for adsorption systems, *J. Hazard. Mater. B* 136 (2006) 681–689.
- [47] S. Azzizian, H. Bashiri, Description of desorption kinetics at the solid/solution interface based on statistical rate theory, *Langmuir* 24 (2008) 13013–13018.
- [48] J. Kou, S. Xu, In situ kinetics and conformation studies of dodecylamine adsorption onto zinc sulfide using quartz crystal microbalance with dissipation (QCM-D), *Colloids Surf. A Physicochem. Eng. Asp.* 490 (2016) 110–120.
- [49] G.W. Kajjumba, S. Emik, A. Ongen, H.K. Ozcan, S. Aydin, Modelling of adsorption kinetic processes—errors, theory and application, in: *Advanced Sorption Process Applications*, IntechOpen, 2018.
- [50] J.T. O'Neal, E.Y. Dai, Y. Zhang, K.B. Clark, K.G. Wilcox, I.M. George, N. E. Ramasamy, D. Enriquez, P. Batsy, M. Sammalkorpi, J.L. Lutkenhaus, QCM-D investigation of swelling behaviour of layer-by-layer thin films upon exposure to monovalent ions, *Langmuir* 34 (2018) 999–1009.
- [51] B.D.E. Raynal, T.E. Hardingham, J.K. Sheehan, D.J. Thornton, Calcium-dependent protein interactions in MUC5B provide reversible cross-links in salivary mucus, *J. Biol. Chem.* 278 (31) (2003) 28703–28710.
- [52] F.G. Oppenheim, E. Salih, W.L. Siqueira, W. Zhang, E.J. Helmerhorst, Salivary proteome and its genetic polymorphisms, *Ann. N. Y. Acad. Sci.* 1098 (2007) 22–50.
- [53] E.C. Veerman, M. Valentijn-Benz, A.V.N. Amerongen, Viscosity of human salivary mucins: effect of pH and ionic strength and role of sialic acid, *J. Biol. Buccale* 17 (4) (1989) 297–306.
- [54] M. Marczynski, K. Jiang, M. Blakeley, V. Srivastava, F. Vilaplana, T. Crouzier, O. Lieleg, Structural alterations of mucins are associated with losses in functionality, *Biomacromolecules* 22 (2021) 1600–1613.
- [55] S.L. Hirsh, D.R. McKenzie, N.J. Nosworthy, J.A. Denman, O.U. Sezerman, M.M. M. Bilek, The Vroman effect: competitive protein exchange with dynamic multilayer protein aggregates, *Colloids Surf. B: Biointerfaces* 103 (2013) 395–404.
- [56] J.B. Madsen, J. Sotres, K.I. Pakkanen, P. Elfer, B. Svensson, M.A. Hachem, T. Arnebrant, S. Lee, Structural and mechanical properties of thin films of bovine submaxillary mucin versus porcine gastric mucin on a hydrophobic surface in aqueous solutions, *Langmuir* 32 (38) (2016) 9687–9696.
- [57] A. Sarkar, F. Xu, S. Lee, Human saliva and model saliva at bulk to adsorbed phases – similarities and differences, *Adv. Colloid Interf. Sci.* 273 (2019) 1–11.
- [58] G.A. Mccubbin, S. Praporski, S. Piantavigna, D. Knappe, R. Hoffman, J.H. Bowie, F. Separovic, L.L. Martin, QCM-D fingerprinting of membrane-active peptides, *Eur. Biophys. J.* 40 (2011) 437–446.
- [59] J. An, A. Dedinaite, A. Nilsson, J. Holgersson, P.M. Claesson, Comparison of a brush-with-anchor and a train-of-brushes mucin on poly(methyl methacrylate) surfaces: adsorption, surface forces, and friction, *Biomacromolecules* 15 (2014) 1515–1525.
- [60] A. Ash, G.R. Burnett, R. Parker, M.J. Ridour, N.M. Rigby, P.J. Wilde, Structural characterisation of parotid and whole mouth salivary pellicles adsorbed onto DPI and QCMD hydroxyapatite sensors, *Colloids Surf. B: Biointerfaces* 116 (2014) 603–611.
- [61] R. Bansil, B.S. Turner, Mucin structure, aggregation, physiological functions and biomedical applications, *Curr. Opin. Colloid Interface Sci.* 11 (2006) 164–170.
- [62] N. Nikoogorgos, J.B. Madsen, S. Lee, Influence of impurities and contact scale on the lubricating properties of bovine submaxillary mucin (BSM) on a hydrophobic surface, *Colloids Surf. B: Biointerfaces* 122 (2014) 760–766.
- [63] K. Riahi, S. Chaabane, B.B. Thayer, A kinetic modelling study of phosphate adsorption onto Phoenix dactylifera L. date palm fibers in batch mode, *J. Saudi Chem. Soc.* 21 (2017) S143–S152.
- [64] S. Xie, Z. Wen, H. Zhan, M. Jin, An experimental study on the adsorption and desorption of Cu(II) in silty clay, *Geofluids Special Issue* (2018) 1–12.
- [65] M. Lundin, T. Sandberg, K.D. Caldwell, E. Blomberg, Comparison of the adsorption kinetics and surface arrangement of “as received” and purified bovine submaxillary gland mucin (BSM) on hydrophilic surfaces, *J. Colloid Interface Sci.* 336 (2009) 30–39.
- [66] L. Wang, J. Li, X. Jiang, Y. Ji, Y. Qu, Y. Zhao, X. Wu, C. Chen, Revealing the binding structure of the protein corona on gold nanorods using synchrotron radiation-based techniques: understanding the reduced damage in cell membranes, *J. Am. Chem. Soc.* 135 (46) (2013) 17359–17368.
- [67] S. Nakata, N. Kido, M. Hayashi, M. Hara, H. Sasabe, T. Sugawara, T. Matsuda, Chemisorption of proteins and their thiol derivatives onto gold surfaces: characterization based on electrochemical nonlinearity, *Biophys. Chem.* 62 (1996) 63–72.
- [68] J. Leal, H.D. Smyth, D. Ghosh, Physicochemical properties of mucus and their impact on transmucosal drug delivery, *Int. J. Pharm.* 532 (1) (2017) 555–572.
- [69] K. Kandori, T. Shimizu, A. Yasukawa, T. Ishikawa, Adsorption of bovine serum albumin onto synthetic calcium hydroxyapatite: influence of particle texture, *Colloids Surf. B: Biointerfaces* 5 (1995) 81–87.
- [70] J.A. Lori, S.Z. Kazare, S.M. Dangoggo, Mechanism for the adsorption of mucin on hydroxyapatite, *Niger. J. Chem. Res.* 10 (2005) 21–29.
- [71] M. Johnsson, M.J. Levine, G.H. Nancollas, Hydroxyapatite binding domains in salivary proteins, *Crit. Rev. Oral Biol. Med.* 4 (3/4) (1993) 371–378.
- [72] X. He, P. Smart, M. Taufiqurrakhman, C. Wang, M. Bryant, Stable oral lubrication enhancer obtained from thiolated polyethylene glycol and mucin, *Friction* (2022) 1–18.
- [73] F. Höök, M. Rodahl, B. Kasemo, P. Brzezinski, Structural changes in hemoglobin during adsorption to solid surfaces: effects of pH, ionic strength, and ligand binding, *Proc. Natl. Acad. Sci. U. S. A.* 95 (1998) 12271–12276.
- [74] J. Klein, Hydration lubrication, *Friction* 1 (1) (2013) 1–23.
- [75] H.Y. Celebioglu, M. Gudjonsdottir, I.S. Chronakis, S. Lee, Investigation of the interaction between mucins and β -lactoglobulin under tribological stress, *Food Hydrocoll.* 54 (Part A) (2016) 57–65.
- [76] P. Bhat, D. Flanagan, M. Donovan, Drug binding to gastric mucus glycoprotein, *Int. J. Pharm.* 134 (1–2) (1996) 15–25.
- [77] A. Ash, P.J. Wilde, D.J. Bradshaw, S.P. King, J.R. Pratten, Structural modifications of the salivary conditioning film upon exposure to sodium bicarbonate: implications for oral lubrication and mouthfeel, *Soft Matter* 12 (2016) 2794–2801.
- [78] A.A. Feiler, A. Sahlholm, T. Sandberg, K.D. Caldwell, Adsorption and viscoelastic properties of fractionated mucin (BSM) and bovine serum albumin (BSA) studied with quartz crystal microbalance (QCM-D), *J. Colloid Interface Sci.* 315 (2) (2007) 475–481.
- [79] J.L. Lanigan, S. Fatima, T.V. Charpentier, A. Neville, D. Dowson, M. Bryant, Lubricious ionic polymer brush functionalised silicone elastomer surfaces, *Biotribology* 16 (2018) 1–9.
- [80] K. Vinke, H.J. Kaper, A. Vissink, P.K. Sharma, Dry mouth: saliva substitutes which adsorb and modify existing salivary condition films improve oral lubrication, *Clin. Oral Investig.* 24 (2020) 4019–4030.
- [81] H. Wan, A. Vissink, P.K. Sharma, Enhancement in xerostomia patient salivary lubrication using a mucoadhesive, *J. Dent. Res.* 99 (8) (2020) 914–921.
- [82] H.-Y. Ren, M. Mizukami, T. Tanabe, H. Furukawa, K. Kurihara, Friction of polymer hydrogels studied by resonance shear measurements, *Soft Matter* 11 (2015) 6192–6200.